Three-Bond C−O−C−C Spin-Coupling Constants in Carbohydrates: Development of a Karplus Relationship

Bidisha Bose,[†] Shikai Zhao,[§] Roland Stenutz,[†] Francis Cloran,[†] Paul B. Bondo,[§] Gail Bondo,[§] Brian Hertz,[†] Ian Carmichael,[‡] and Anthony S. Serianni*,[†]

Contribution from the Department of Chemistry and Biochemistry, and Radiation Laboratory, University of Notre Dame, Notre Dame, Indiana 46556, and Omicron Biochemicals, Inc., 1347 N. Ironwood Drive, South Bend, Indiana 46615

Received April 3, 1998. Revised Manuscript Received July 23, 1998

Abstract: A range of ^{13}C-labeled carbohydrates containing C−O−C−C coupling pathways having different structures and dihedral angles has been prepared and used to identify structural factors affecting $^3J_{COCC}$, especially those across the *O*-glycosidic linkages of oligosaccharides. Model mono- and disaccharides were geometrically optimized using density functional methods, and scalar couplings involving carbon were calculated using a similar approach coupled with finite-field perturbation theory. Experimental and calculated $^3J_{COCC}$ values were in close agreement, thus allowing use of the latter to better define the effect of carbohydrate structure on $^3J_{COCC}$ magnitude. In addition to dihedral angle, the disposition of terminal electronegative substituents along the C−O−C−C coupling pathway significantly affects $^3J_{COCC}$ values, and structural motifs have been identified where these effects may be encountered in oligosaccharides. A simple Karplus equation for trans-*O*-glycoside $^3J_{COCC}$ values is proposed and has been applied in the reanalysis of trans-*O*-glycosidic couplings in ^{13}C-labeled methyl β-lactoside and sucrose. The behavior of trans-*O*-glycosidic $^2J_{COC}$ and $^3J_{COCH}$ values, which provide structural information complementary to that derived from $^3J_{COCC}$ values, is also discussed.

Introduction

Conformational analysis of oligosaccharides is based largely on the observation of inter-residue ^{1}H−^{1}H NOEs to assess the torsional preferences about their constituent *O*-glycosidic linkages. In many instances, however, the number of measurable NOEs is smaller than needed to establish solution conformation with reasonable certainty.[1] In addition, the interpretation of NOEs is complex if conformational flexibility exists, due to the r^{-6} dependence of NOE on ^{1}H−^{1}H internuclear distance.[2] Consequently, the measurement of complementary NMR parameters, such as $^3J_{COCH}$, $^2J_{COC}$, and $^3J_{COCC}$ values, that may be sensitive to linkage conformation and more readily interpreted than ^{1}H−^{1}H NOEs in flexible systems, is desirable.

$^3J_{COCH}$ values have been measured to assess the phi (ϕ) and psi (ψ) torsion angles of oligosaccharides (Scheme 1),[3−5] and Karplus relationships have been reported for this vicinal coupling.[6,7] A "projection-resultant" method has been described recently which correlates $^2J_{COC}$ magnitude and sign to *O*-glycosidic linkage conformation,[8a] and its general features have been confirmed using triply-[^{13}C]-labeled model compounds and ^{13}C−^{13}C COSY-45.[8b,c] In contrast, little effort has been devoted to establishing a relationship between $^3J_{COCC}$ magnitude and molecular torsion angles in carbohydrates, despite its apparent importance, although preliminary reports have appeared recently.[9] Of the six spin-couplings available across *O*-glycosidic linkages (excluding linkages involving primary hydroxyl groups), three are $^3J_{COCC}$ values, and thus, substantial information might be gleaned from their interpretation (Scheme 1).

Scheme 1

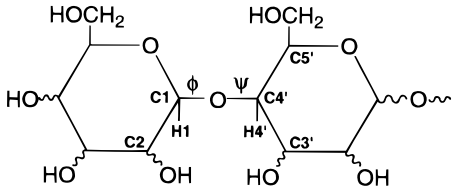

$^3J_{CC}$ values are affected by factors in addition to dihedral angle,[10−16] and efforts to apply $^3J_{COCC}$ to assess *O*-glycosidic linkage conformation must address these secondary factors. We present herein experimental and computational studies aimed at providing a reliable correlation between molecular structure, conformation, and $^3J_{COCC}$ magnitude in saccharides.

Experimental Section

Synthesis of ^{13}C-Labeled Compounds. D-[1-^{13}C]Arabinose was prepared from D-erythrose, and D-[1-^{13}C]galactose and D-[1-

* Author for correspondence.
[†] Department of Chemistry and Biochemistry, University of Notre Dame.
[‡] Radiation Laboratory, University of Notre Dame.
[§] Omicron Biochemicals, Inc.

(1) Homans, S. W. *Prog. NMR Spectrosc.* **1990**, *22*, 55−81.
(2) Jardetzky, O. *Biochim. Biophys. Acta* **1980**, *621*, 227−232.
(3) (a) Nunez, H. A.; Barker, R. *Biochemistry* **1980**, *19*, 489−495. (b) Hamer, G. K.; Balza, F.; Cyr, N.; Perlin, A. S. *Can. J. Chem.* **1978**, *56*, 3109−3116. (c) Parfondry, A.; Cyr, N.; Perlin, A. S. *Carbohydr. Res.* **1977**, *59*, 299−309. (d) Walker, T. E.; London, R. E.; Whaley, T. W.; Barker, R.; Matwiyoff, N. A. *J. Am. Chem. Soc.* **1976**, *98*, 5807−5813. (e) Schwarcz, J. A.; Perlin, A. S. *Can. J. Chem.* **1972**, *50*, 3667−3676.
(4) Hayes, M. L.; Serianni, A. S.; Barker, R. *Carbohydr. Res.* **1982**, *100*, 87−101.
(5) Duker, J.; Serianni, A. S. *Carbohydr. Res.* **1993**, *249*, 281−303.
(6) Tvaroska, I.; Hricovini, H.; Petrakova, E. *Carbohydr. Res.* **1989**, *189*, 359−362.
(7) Mulloy, B.; Frenkiel, T. A.; Davies, D. B. *Carbohydr. Res.* **1988**, *184*, 39−46.
(8) (a) Church, T.; Carmichael, I.; Serianni, A. S. *Carbohydr. Res.* **1996**, *280*, 177−186. (b) Serianni, A. S.; Bondo, P. B.; Zajicek, J. *J. Magn. Reson. Series B* **1996**, *112*, 69−74. (c) Zhao, S.; Bondo, G.; Zajicek, J.; Serianni, A. S. *Carbohydr. Res.*, **1998**, *309*, 145−152.
(9) (a) Milton, M. J.; Harris, R.; Probert, M. A.; Field, R. A.; Homans, S. W. *Glycobiology* **1998**, *8*, 147−153. (b) Xu, Q.; Bush, C. A. *Carbohydr. Res.* **1998**, *306*, 335−339.

10.1021/ja981127f CCC: $15.00
Published on Web 10/16/1998

^{13}C]talose were prepared from D-lyxose, by cyanohydrin reduction using K^{13}CN (99 atom %, Cambridge Isotope Laboratories).[17−19] D-[6-^{13}C]Aldohexoses were prepared as described by Wu et al.[20]

L-[1-^{13}C]Fucose (6-deoxy-L-[1-^{13}C]galactose) and 6-deoxy-L-[1-^{13}C]talose were prepared from 5-deoxy-L-lyxose. L-Fucose (Sigma) was treated with two equivalents of $Pb(OAc)_4$ to yield 4-deoxy-L-threose.[21] The latter deoxytetrose was converted to 5-deoxy-L-lyxose and -xylose by treatment with KCN followed by cyanohydrin reduction.[21] The epimeric deoxypentose mixture was separated by chromatography on Dowex 50 × 8 (200−400 mesh) in the Ca^{2+} form,[19] with the *xylo* isomer eluting first. 5-Deoxy-L-lyxose was treated with K^{13}CN, and the resulting epimeric aldononitriles were reduced catalytically[17,18] to give L-[1-^{13}C]fucose and 6-deoxy-L-[1-^{13}C]talose. These epimeric 6-deoxyhexoses were separated by chromatography on Dowex 50 × 8 (200−400 mesh) ion-exchange resin in the Ca^{2+} form,[19] with the *galacto* isomer eluting first.

L-[1-^{13}C]Rhamnose was prepared from 5-deoxy-L-arabinose[21] and K^{13}CN by cyanohydrin reduction.[17,18] The *gluco* isomer eluted first on Dowex 50 × 8 (200−400 mesh) in the Ca^{2+} form.[19] 3-Deoxy-D-[1-^{13}C]glucose and 3-deoxy-D-[1-^{13}C]mannose were prepared from 2-deoxy-D-ribose (2-deoxy-D-*erythro*-pentose, Sigma) and K^{13}CN by cyanohydrin reduction as described for the preparation of D-[1-^{13}C]glucose.[17,18] The 3-deoxyhexose epimers were separated by chromatography on a column (4.5 cm × 110 cm) containing Dowex 50 × 8 (200−400 mesh) ion-exchange resin in the Ba^{2+} form,[22] with the *gluco* epimer eluting first.

6-Deoxy-D-[6-^{13}C]glucose was prepared from D-[6-^{13}C]glucose[23] as follows. Methyl 6-*O*-*p*-toluenesulfonyl-α-D-[6-^{13}C]-glucopyranoside (0.88 g, 2.5 mmol, prepared as described below) was dissolved in THF (10 mL) and the solution was added to a suspension of lithium aluminum hydride (0.32 g, 8.4 mmol) in THF (20 mL). The mixture was stirred at room temperature for 10 h, and then ethyl acetate (1.5 mL) and water (0.75 mL) were added slowly. The mixture was filtered and the filtrate concentrated at 30 °C in vacuo. The residue was dissolved in aqueous H_2SO_4 (0.1% v/v, 10 mL), and the solution was refluxed for 3 h. After cooling, the solution was deionized with batchwise and consecutive additions of Dowex 50 × 8 (20−50 mesh) (H^+) and Dowex 1 × 8 (20−50 mesh) (OAc^-) ion-exchange resins, and the deionized solution was concentrated to ∼5 mL at 30 °C in vacuo and applied to a column (4.4 cm × 104 cm) containing Dowex 50 × 8 (200−400 mesh) ion-exchange resin in the Ca^{2+} form.[19] Elution with distilled water gave 6-deoxy-D-[6-^{13}C]glucose (0.29 g, 1.7 mmol, 68%) as a clear syrup.

D-[1-^{13}C]-, [2-^{13}C]-, [3-^{13}C]-, and [6-^{13}C]Fructose were prepared from D-[1-^{13}C]-,[17,18] [2-^{13}C]-,[24] [3-^{13}C]-,[17,18,24−26] and [6-^{13}C]glucose[23] by treatment with D-xylose (D-glucose) isomerase,[27] followed by purification of the *gluco*−*fructo* mixture by chromatography.[18] D-[1-^{13}C]Tagatose was prepared from D-[1-^{13}C]galactose by base isomerization in the presence of phenylboronic acid (PBA).[28,29] D-[1-^{13}C]Galactose (1.9 g, 10.5 mmol) was dissolved in 34 mL of distilled water, the solution was cooled to 10 °C in an ice-bath, and phenylboronic acid (1.4 g, 11.5 mmol) was added. The resulting solution was adjusted to pH 12.8 with 2 M KOH, and the solution was incubated at 30−37 °C for 24 h. The reaction was quenched with the addition of Dowex 50 × 8 (20−50 mesh) ion-exchange resin in the H^+ form until the pH dropped to 2.8, and the solution was transferred to a separatory funnel and extracted three times with ethyl ether to remove the PBA. The aqueous phase was then deionized with batchwise and successive additions of excess Dowex 50 × 8 (20−50 mesh) (H^+) and Dowex 1 × 8 (20−50) (OAc^-) ion-exchange resins. The deionized solution was concentrated in vacuo to ∼2 mL and applied to a column (10 cm × 100 cm) containing Dowex 50 × 8 (200−400 mesh) ion-exchange resin in the Ca^{2+} form.[19] D-[1-^{13}C]Galactose (0.8 g, 4.4 mmol) eluted first, followed by D-[1-^{13}C]tagatose (1.0 g, 5.5 mmol) and D-[1-^{13}C]talose (0.07 g, 0.4 mmol). D-[2-^{13}C]-Tagatose was prepared similarly from D-[2-^{13}C]galactose.[24]

L-[4-^{13}C] and [5-^{13}C]Sorbose were prepared from dihydroxyacetone phosphate and DL-[1-^{13}C]glyceraldehyde[30] or DL-[2-^{13}C]-glyceraldehyde[30] using rabbit muscle fructose 6-phosphate aldolase (Sigma).[31]

L-[6-^{13}C]Sorbose was prepared from L-[6-^{13}C]idose by base isomerization in the presence of phenylboronic acid.[28,29] A 0.22 M solution of L-[6-^{13}C]idose in water (10 mL) was chilled to 10 °C, and 0.30 g phenylboronic acid was added. The pH was adjusted to ∼11 with the addition of saturated K_2CO_3 and then to pH ∼13 with 50% NaOH. The flask was flushed with N_2 and stirred at room temperature for 42 h. The pH was then lowered to ∼2 with the addition of Dowex 50 × 8 (20−50 mesh) (H^+) ion-exchange resin. After being filtered, the solution was extracted (3×) with 50 mL portions of $CHCl_3$ to remove the phenylboronic acid, and the resulting solution was decolorized with charcoal. Crystals of D-[6-^{13}C]sorbose (0.17 g, 0.94 mmol, 43%) formed when the solution was concentrated in vacuo. The resulting crystals were dissolved in a minimum volume of water, and the solution was loaded on a column (4.5 cm × 110 cm) containing Dowex 50 × 8 (200−400 mesh) (Ba^{2+});[22] elution with water gave pure L-[6-^{13}C]sorbose (124

(10) Marshall, J. L. *Carbon-Carbon and Carbon-Proton NMR Couplings: Applications to Organic Stereochemistry and Conformational Analysis. Methods in Stereochemical Analysis*; Verlag Chemie International: Deerfield Beach, 1983; Vol. 2.
(11) Marshall, J. L.; Conn, S. A.; Barfield, M. *Org. Magn. Reson.* **1977**, *9*, 404−407.
(12) Barfield, M.; Conn, S. A.; Marshall, J. L.; Miiller, D. E. *J. Am. Chem. Soc.* **1976**, *98*, 6253- 6260.
(13) Barfield, M.; Burfitt, I.; Doddrell, D. *J. Am. Chem. Soc.* **1975**, *97*, 2631−2634.
(14) Wray, V. *Prog. NMR Spectrosc.* **1979**, *13*, 177−256.
(15) Marshall, J. L.; Miiller, D. E. *J. Am. Chem. Soc.* **1973**, *95*, 8305−8308.
(16) Barfield, M.; Marshall, J. L.; Canada, E. D.; Willcott, M. R., III. *J. Am. Chem. Soc.* **1978**, *100*, 7075−7077.
(17) Serianni, A. S.; Nunez, H. A.; Barker, R. *Carbohydr. Res.* **1979**, *72*, 71−78.
(18) Serianni, A. S.; Vuorinen, T.; Bondo, P. B. *J. Carbohydr. Chem.* **1990**, *9*, 513−541.
(19) Angyal, S. J.; Bethell, G. S.; Beveridge, R. *Carbohydr. Res.* **1979**, *73*, 9−18.
(20) Wu, J.; Bondo, P. B.; Vuorinen, T.; Serianni, A. S. *J. Am. Chem. Soc.* **1992**, *114*, 3499−3505.
(21) Snyder, J. R.; Serianni, A. S. *Carbohydr. Res.* **1987**, *163*, 169−188.
(22) Jones, J. K. N.; Wall, R. A. *Can. J. Chem.* **1960**, *38*, 2290−2294.
(23) King-Morris, M. J.; Bondo, P. B.; Mrowca, R. A.; Serianni, A. S. *Carbohydr. Res.* **1988**, *175*, 49−58.
(24) Hayes, M. L.; Pennings, N. J.; Serianni, A. S.; Barker, R. *J. Am. Chem. Soc.* **1982**, *104*, 4, 6764−6769.
(25) Kline, P. C.; Serianni, A. S. *J. Am. Chem. Soc.* **1990**, *112*, 7373−7381.
(26) Serianni, A. S.; Bondo, P. B. *J. Biomol. Struct. Dyn.* **1994**, *11*, 1133−1148.
(27) Walker, T. E.; Unkefer, C. J.; Ehler, D. S. *J. Carbohydr. Chem.* **1988**, *7*, 115−132.
(28) Barker, S. A.; Chopra, A. K.; Hatt, B. W.; Somers, P. J. *Carbohydr. Res.* **1973**, *26*, 33−40.
(29) Barker, S. A.; Hatt, B. W.; Somers, P. J. *Carbohydr. Res.* **1973**, *26*, 41−53.
(30) Serianni, A. S.; Clark, E. L.; Barker, R. *Carbohydr. Res.* **1979**, *72*, 79−91.
(31) Serianni, A. S.; Cadman, E.; Pierce, J.; Hayes, M. L.; Barker, R. *Methods Enzymol.* **1982**, *89*, Part D, 83−92.

mg, 0.68 mmol, 31%). The starting material in this synthesis, L-[6-^{13}C]idose, was prepared from 1,2-*O*-isopropylidene-D-*xylo*-dialdopentofuranose and K^{13}CN as described by King-Morris et al.[23]

Ethyl α- and β-D-[1-^{13}C]- and [2-^{13}C]gluco- and mannopyranosides were prepared from D-[1-^{13}C]glucose and mannose[17,18] and D-[2-^{13}C]glucose and mannose[24] by Fischer glycosidation in ethanol, using Dowex 50 × 8 (200−400 mesh) (H^+) ion-exchange resin as the catalyst.[32] The resulting glycoside mixtures (mainly pyranosides) were separated by chromatography on Dowex 1 × 2 (200−400 mesh) in the OH^- form.[33] Isopropyl α- and β-D-[1-^{13}C]- and [2-^{13}C]gluco- and mannopyranosides were prepared similarly using 2-propanol as the solvent.

Methyl β-D-[1-^{13}C]ribofuranoside was prepared from D-[1-^{13}C]ribose,[25,26] and methyl α- and β-D-fructofuranosides (singly ^{13}C-labeled at C1, C2, and C3) were prepared from the corresponding labeled fructoses.[5]

Methyl 3,6-anhydro-α-D-[1-^{13}C]glucopyranoside and methyl 3,6-anhydro-β-D-[1-^{13}C]glucopyranoside were prepared as follows. Anhydrous pyridine (5 mL) was added to a mixture of methyl α-D-[1-^{13}C]glucopyranoside[32] (0.43 g, 2.2 mmol) and *p*-toluenesulfonyl chloride (0.41 g, 2.2 mmol) at 0 °C under nitrogen, and the mixture was stirred at room temperature for 2 days. The pyridine was then removed by distillation under vacuum. The residue was dissolved in CH_2Cl_2 (50 mL), and the resulting solution was extracted with saturated $NaHSO_4$ (10 mL) and saturated $NaHCO_3$ (10 mL), dried over Na_2SO_4, and concentrated to give a colorless solid. The solid was washed several times with ether until it appeared homogeneous by TLC, giving methyl 6-*O*-*p*-toluenesulfonyl-α-D-[1-^{13}C]glucopyranoside as a colorless solid (0.17 g, 0.49 mmol, 22%). All of this product was dissolved in MeOH (2 mL) and aqueous NaOH (1 M, 1 mL), and the mixture was stirred at room temperature for 2 days and then neutralized with the addition of dry ice. The solution was concentrated at 30 °C in vacuo to give a colorless solid. Acetone (10 mL) was added, and the suspension was stirred at 40 °C for 30 min, filtered, and concentrated at 30 °C in vacuo to give solid methyl 3,6-anhydro-α-D-[1-^{13}C]glucopyranoside (0.09 g, 0.45 mmol, 92%). Methyl 3,6-anhydro-β-D-[1-^{13}C]glucopyranoside was prepared in a similar fashion from methyl β-D-[1-^{13}C]glucopyranoside.[32]

4,6-*O*-Ethylidene-D-[1-^{13}C]glucose was prepared from D-[1-^{13}C]glucose[17,18] and acetaldehyde.[34] A solution of 50 μL of concentrated H_2SO_4 in 0.3 mL CH_3CHO (5.4 mmol) was added to 1.0 g of D-[1-^{13}C]glucose (5.5 mmol). After the mixture was stirred for 16 h, the thick paste was extracted with boiling EtOAc (3 × 50 mL) to give 0.28 g of 4,6-*O*-ethylidene-D-[1-^{13}C]glucose (1.3 mmol, 24%). Unreacted D-[1-^{13}C]glucose (∼0.7 g) was recovered from the resulting extracted residue.

4,6-*O*-Ethylidene-D-[1-^{13}C]galactose was prepared from D-[1-^{13}C]galactose and acetaldehyde as described above for 4,6-*O*-ethylidene-D-[1-^{13}C]glucose. Extraction with boiling EtOAc gave 0.19 g (0.90 mmol, 16%) of the protected hexose; 0.87 g of unreacted D-[1-^{13}C]galactose was recovered.

^{13}C-Labeled sucrose was prepared enzymically,[5] and α-D-[1-^{13}C]*erythro*- and α-D-[1-^{13}C]*threo*-2-pentulofuranoses were prepared as described by Vuorinen and Serianni.[35]

NMR Spectroscopy. NMR spectra were obtained on a Varian Unity*Plus* 600 MHz NMR spectrometer operating at 599.888 MHz for ^{1}H and 150.852 MHz for ^{13}C. One-dimensional ^{1}H and ^{13}C NMR spectra were collected on ∼20 mM and ∼100 mM aqueous (^2H_2O) solutions, respectively, at 30 °C using a conventional 5 mm broadband probe or a 3 mm dual ^{1}H−^{13}C microprobe (Nalorac). Spectra were processed with resolution enhancement (sine-bell) to facilitate the measurement of small couplings (≥0.6 Hz).

Calculational Methods. All calculations were performed with a modified[36] version of the Gaussian 94 suite of programs.[37] Electron correlation effects were treated by means of density functional theory. The standard B3LYP functional, described by Becke,[38] was used throughout. This functional comprises both local[39] and nonlocal[40] exchange contributions and also contains terms accounting for local[41] and nonlocal[42] correlation corrections.

Geometrical optimization employed the B3LYP functional together with the standard 6-31G* basis set.[43] Indirect spin−spin coupling constants in the optimized structures were determined using a previously constructed basis set[36] by finite (Fermi contact)-field double perturbation theory.[44] Suitable values for the perturbing fields for the various couplings were chosen to ensure sufficient numerical precision, while still allowing a satisfactory low-order finite-difference representation of the effect of the perturbation. Only the Fermi contact component of each coupling constant was considered.

Results and Discussion

1. Defining and Delimiting the Problem. $^3J_{COCC}$ values have been measured previously across the *O*-glycosidic linkages of ^{13}C-labeled oligosaccharides, and conformational interpretations have been offered, despite the lack of a thorough understanding of the structural factors affecting their magnitudes.[3a,4,5] Some experimental evidence has been reported, suggesting that $^3J_{COCC}$ obeys a Karplus relationship similar to that observed for $^3J_{HH}$,[45] $^3J_{CH}$,[6,7,46,47] and other vicinal spin-coupling constants.[9,10] However, the precise form of this relationship, that is, the shape and amplitude of the Karplus curve, is unknown. Defining this relationship in the context of oligo- and polysaccharide structure is not straightforward, since, like $^3J_{HH}$ values,[45] $^3J_{CC}$ values are influenced by factors in addition to dihedral angle. These factors include the presence or absence of electronegative substituents *within* the coupling pathway (e.g., C−C−C−C vs C−O−C−C) or *appended to* pathway atoms

(32) Podlasek, C. A.; Wu, J.; Stripe, W. A.; Bondo, P. B.; Serianni, A. S. *J. Am. Chem. Soc.* **1995**, *117*, 8635−8644.
(33) Austin, P. W.; Hardy, F. E.; Buchanan, J. C.; Baddiley, J. *J. Chem. Soc.* **1963**, 5350−5353.
(34) Perlin, A. S. *Methods Carbohydr. Chem.* **1962**, *1*, 64−66.
(35) Vuorinen, T.; Serianni, A. S. *Carbohydr. Res.* **1990**, *209*, 13−31.
(36) Carmichael, I. *J. Phys. Chem.* **1993**, *97*, 1789−92.
(37) Frisch, M. J.; Trucks, G. W.; Schlegel, H. B.; Gill, P. M. W.; Johnson, B. G.; Robb, M. A.; Cheeseman, J. R.; Keith, T.; Petersson, G. A.; Montgomery, J. A.; Raghavachari, K.; Al-Laham, M. A.; Zakrzewski, V. G.; Ortiz, J. V.; Foresman, J. B.; Peng, C. Y.; Ayala, P. Y.; Chen, W.; Wong, M. W.; Andres, J. L.; Replogle, E. S.; Gomperts, R.; Martin, R. L.; Fox, D. J.; Binkley, J. S.; Defrees, D. J.; Baker, J.; Stewart, J. P.; Head-Gordon, M.; Gonzalez, C.; Pople, J. A. *Gaussian 94*; Gaussian, Inc.: Pittsburgh, PA, 1995.
(38) Becke, A. D. *J. Chem. Phys.* **1993**, *98*, 5648−52.
(39) Slater, J. C. *The Self-Consistent Field for Molecules and Solids*; McGraw-Hill: New York, 1974.
(40) Becke, A. D. ACS Symposium Series; American Chemical Society: Washington, DC, 1989; p 165.
(41) Vosko, S. H.; Wilk, L.; Nusair, M. *Can. J. Phys.* **1980**, *58*, 1200.
(42) Lee, C.; Yang, W.; Parr, R. G. *Phys Rev. B* **1988**, *37*, 785.
(43) Hehre, W. J.; Ditchfield, R.; Pople, J. A. *J. Chem. Phys.* **1972**, *56*, 2257−61.
(44) Kowalewski, J.; Laaksonen, A.; Roos, B.; Siegbahn, P. *J. Chem. Phys.* **1979**, *71*, 2896−902.
(45) (a) Haasnoot, C. A. G.; de Leeuw, F. A. A. M.; Altona, C. *Tetrahedron* **1980**, *36*, 2783−2792. (b) van Wijk, J.; Huckriede, B. D.; Ippel, J. H.; Altona, C. *Methods Enzymol.* **1992**, *211*, Part A, 286−306.
(46) Schwarcz, J.; Perlin, A. S. *Can. J. Chem.* **1972**, *50*, 3667−3676.
(47) Spoormaker, T.; de Bie, M. J. A. *Recl. Trav. Chim. Pays-Bas* **1978**, *97*, 85−87.

Scheme 2

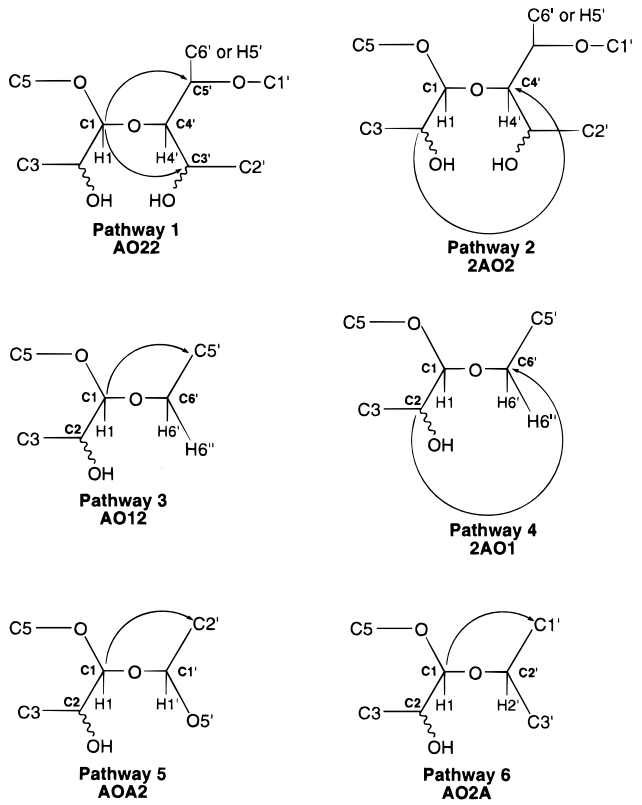

(e.g., HO−C−O−C−C vs H−C−O−C−C), and their disposition with respect to the pathway.

Six structurally distinct pathways are possible in oligosaccharides containing simple aldoses (Scheme 2). Each pathway can be identified using a four-element symbolism where A = anomeric carbon, O = oxygen, 2 = secondary alcohol carbon, and 1 = primary alcohol carbon. Thus, for example, coupling between C1 and C5′ in a (1→4)-linked disaccharide such as methyl β-lactoside **1** is defined as an AO22 pathway, whereas

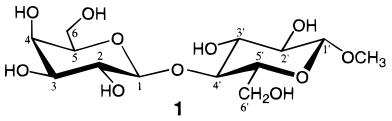

1

coupling between C2 and C4′ in **1** is defined as a 2AO2 pathway (Scheme 2). In this investigation, coupling behavior in AO22, 2AO2, AO12, and 2AO1 pathways is examined. It should be noted that the AO22 and AO12 pathways and the 2AO2 and 2AO1 pathways are structurally related, differing only in a single substitution of an internal or terminal alcohol carbon in the coupling pathway.

Two model systems (Scheme 3) mimic Pathways 1−4 (Scheme 2). The C1−O5−C5−C6 coupling pathway in aldohexopyranosyl rings is an AO21 pathway, which approximates the AO22 and AO12 pathways in Scheme 2. Likewise, the C1−C2−O6−C6 coupling pathway in ketohexopyranosyl rings is a 1AO1 pathway, which mimics the 2AO2 and 2AO1 pathways in Scheme 2. The use of these pathway mimics serves as a controllable means to estimate the coupling behavior in actual coupling pathways in oligosaccharides.

2. Substituent Effects on $^3J_{CC}$ Values in Aldohexopyranosyl Rings. An assessment of substitution effects on $^3J_{CC}$ in carbohydrates can be made by comparing couplings in structures that are conformationally homogeneous. The aldopyranoses

Scheme 3

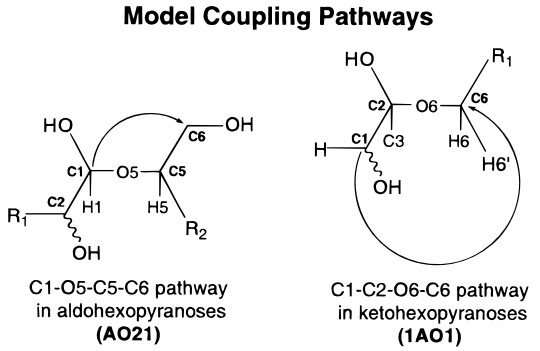

Scheme 4

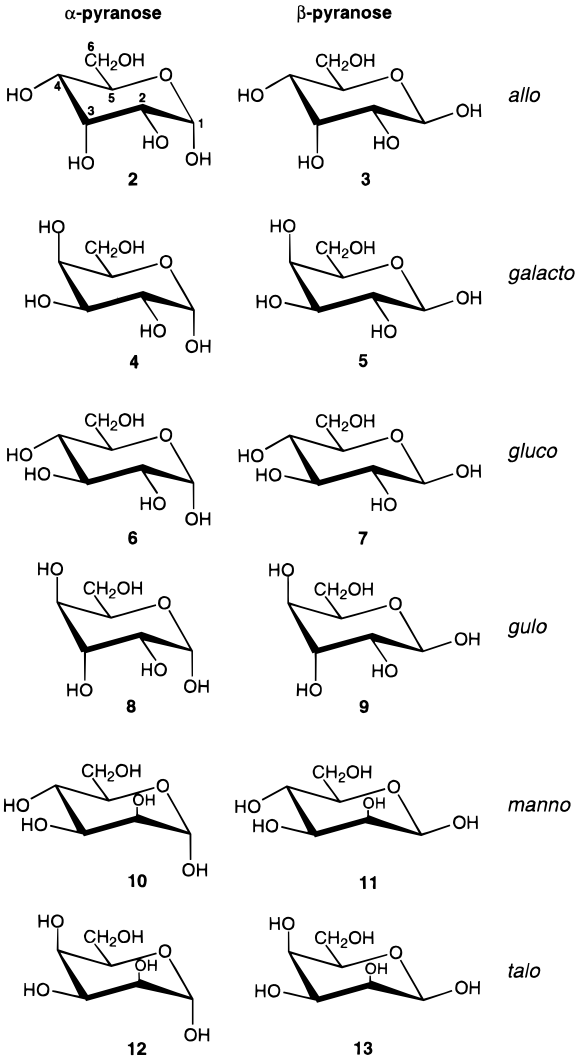

discussed below (Scheme 4) prefer the $^4C_1$ conformation in solution, although the extent of this preference depends on ring configuration (Table 1).

$^3J_{C1,C6}$ and $^3J_{C3,C6}$ values were measured in several simple [6-^{13}C]aldohexopyranoses (Table 1). Their signs were found to be positive,[8b] and we assume in the following discussion that all of the $^3J_{CC}$ values are positive in sign. $^3J_{C1,C6}$ in aldohexopyranosyl rings may be affected by at least four structural variables (Scheme 5), and experimental assessments of three of these factors, namely, configuration at C1, C−O−C−C torsion angle, and hydroxymethyl conformation, are provided below. Similar structural factors also influence $^3J_{C3,C6}$; in this

Table 1. $^3J_{C1,C6}$ and $^3J_{C3,C6}$ Values[a] in Some D-Aldohexopyranoses

aldohexopyranose	$^3J_{C1,C6}$	$^3J_{C3,C6}$	ΔE[b]
α-D-*allo* **2**	3.2	2.8	1.41[c]
α-D-*galacto* **4**	3.6	3.7	5.65
α-D-*gluco* **6**	3.3	3.9	5.20
α-D-*gulo* **8**	3.4	1.8	0.84[c]
α-D-*manno* **10**	3.3	3.6	4.24
α-D-*talo* **12**	3.4	3.4	3.69
β-D-*allo* **3**	3.4	3.0	3.91
β-D-*galacto* **5**	4.5	4.1	6.80
β-D-*gluco* **7**	4.2	4.4	6.51
β-D-*gulo* **9**	3.7	1.8	3.60
β-D-*manno* **11**	3.9	4.2	6.86
β-D-*talo* **13**	4.3	3.8	7.37

[a] In Hz, ±0.1 Hz; ^2H_2O solvent, ~21 °C. Data taken from ref 20. Both $^3J_{C1,C6}$ and $^3J_{C3,C6}$ are positive in sign.[8b] [b] Difference in energy (in kcal/mol) between the most stable $^4C_1$ conformer and the next most stable conformer computed using the MM3(92) program, as reported in ref 76. [c] The relatively small values of ΔE in **2** and **8** indicate that the $^1C_4$ form is relatively stable and, thus, that the *J* values in **2** and **8** may not be reliably attributed to a single ($^4C_1$) conformer.

Scheme 5

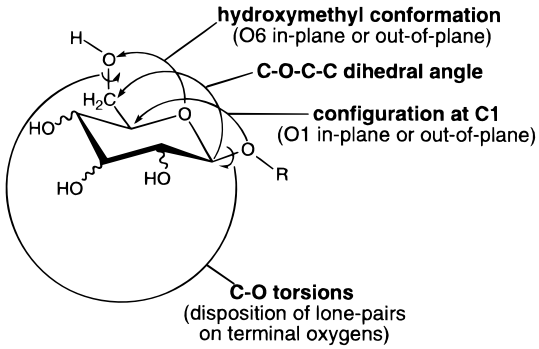

case, substitution effects at the intervening C4 carbon must also be considered.

In the six α-D-aldohexopyranoses studied (Scheme 4), $^3J_{C1,C6}$ values are smaller (3.4 ± 0.1 Hz) than those in the corresponding *β*-D-aldohexopyranoses (4.0 ± 0.4 Hz) despite that fact that these couplings *in both* α- and *β*-pyranoses relate to C−O−C−C dihedral angles near 180°. This result suggests that, in addition to dihedral angle, the orientation of O1 with respect to the C1−O5−C5−C6 coupling pathway is an important determinant of $^3J_{C1,C6}$. An in-plane (W-shaped) orientation, as found in the *β*-pyranoses, makes a *positive* contribution to the coupling. However, exceptions to this trend are observed, suggesting that other factors are at work (see below); for example, $^3J_{C1,C6}$ in **2** (3.2 Hz) is very similar to $^3J_{C1,C6}$ in **3** (3.4 Hz).

While the orientation of O1 with respect to the C1−O5−C5−C6 coupling pathway is an important determinant of $^3J_{C1,C6}$ in **2**−**13** (in addition to the C1−O5−C5−C6 dihedral angle), the influence of O6 on this coupling cannot be ignored. In 4,6-*O*-ethylidene-D-[1-^{13}C]glucopyranoses **14** and galactopyranoses **15** (Table 2), the C1−O5−C5−C6 torsion angle is ~180°, whereas the O5−C5−C6−O6 torsion angles differ. In **14**, the

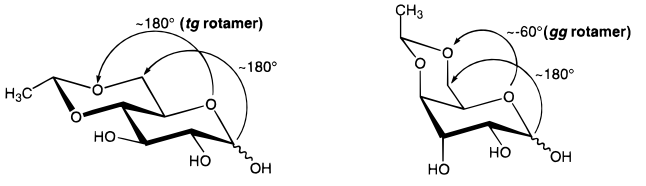

4,6-*O*-ethylidene-D-glucopyranoses **14** 4,6-*O*-ethylidene-D-galactopyranoses **15**

latter angle is ~180°, corresponding to the *tg* rotamer (Scheme 6), whereas in **15** this angle is ~−60°, corresponding to the *gg* rotamer. $^3J_{C1,C6}$ values in **6** (3.3 Hz) and **7** (4.2 Hz) (Table 1)

Table 2. J_{CC} Values[a] in D-[1-^{13}C]Galactopyranoses, [1-^{13}C]Deoxyaldohexopyranoses, and 4,6-*O*-Ethylidene-D-[1-^{13}C]aldohexopyranoses

aldopyranose	$^1J_{C1,C2}$	$^2J_{C1,C3}$	$^2J_{C1,C5}$	$^{3+3}J_{C1,C4}$	$^3J_{C1,C6}$[b]
α-D-*galacto* **4**	46.0	nc	−1.9	nc	3.6
α-L-*fuco* **16**	45.9	nc	−2.0	nc	3.0[d]
α-L-*rhamno* **18**	46.7	nc	−2.0	0.7	3.2
6-deoxy-α-L-*talo* **20**					3.1
β-D-*galacto* **5**	45.9	+4.6	nc	nc	4.5
β-L-*fuco* **17**	45.7	+4.6	nc	nc	4.2
β-L-*rhamno* **19**	42.6	+3.9	nc	nc	3.9
6-deoxy-*β*-L-*talo* **21**					4.0
4,6-*O*-ethylidene-α-*gluco* **14**α	45.8	nc	−1.7	nc	4.1
4,6-*O*-ethylidene-*β*-*gluco* **14***β*	45.7	+4.0	nc	nc	4.9
4,6-*O*-ethylidene-α-*galacto* **15**α	45.8	nc	−2.1	nc	3.4
4,6-*O*-ethylidene-*β*-*galacto* **15***β*	46.0	+4.9	nc	nc	4.2
2-deoxy-α-D-*arabino*-hexopyranose **24**	40.7	−2.3	−2.1	nc	3.2
2-deoxy-*β*-D-*arabino*-hexopyranose **25**	40.3	+1.8	nc	nc	4.1
3-deoxy-α-D-glucopyranose **26**	46.7	−2.0	−2.0	nc	3.0
3-deoxy-*β*-D-glucopyranose **27**	46.8	+1.0	0.9[e]	nc	3.5
3-deoxy-α-D-mannopyranose **28**	47.2	−1.8	−2.0	1.8	2.8
3-deoxy-*β*-D-mannopyranose **29**	43.4	+1.1[c]	0.4[e]	1.6	3.1

[a] In Hz, ±0.1 Hz; ^2H_2O solvent, ~21 °C; nc = no coupling observed (J < 0.5 Hz). Data for **4** and **5** were taken from ref 71. Signs of the two-bond couplings were predicted using the projection resultant method.[8a] [b] $^3J_{C1,C6}$ values in **16** and **17** were reported previously to be identical;[3d,72] however, present measurements revealed different values due to the improved resolution of the closely spaced C6 doublets at 150 MHz. [c] Value not unequivocal due to possible misassignment of the C3 signal in **29**. [d] Value ±0.3 Hz. [e] Sign unknown.

Scheme 6

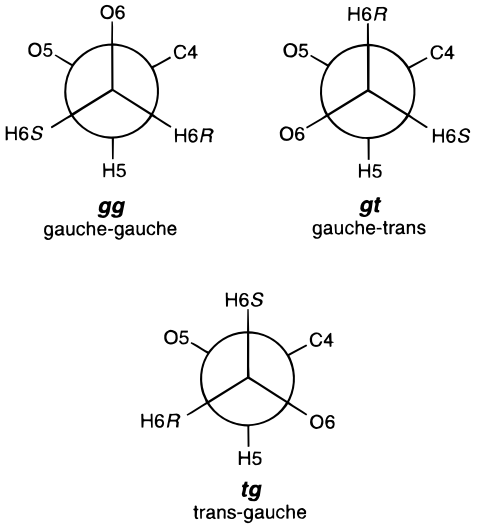

are ~0.8 Hz *smaller* than $^3J_{C1,C6}$ values in corresponding anomers of **14**, thus showing that the in-plane orientation of O6 enhances coupling. In contrast, $^3J_{C1,C6}$ values in **4** (3.6 Hz) and **5** (4.5 Hz) are ~0.2 Hz *larger* than $^3J_{C1,C6}$ values in the corresponding anomers of **15**; the small proportion of *tg* rotamer,[48] which is not present in **15**, is responsible for the enhanced coupling in **4** and **5**.

On the basis of the above considerations, the enhanced $^3J_{C1,C6}$ values observed in *β*-pyranoses relative to α-pyranoses (Table 1) could be attributed, *in part*, to differences in conformation about the C5−C6 bond. However, given that the population of the *tg* rotamer (which places O6 in the C1−O5−C5−C6 coupling plane) is not expected to differ significantly between pyranose anomers,[48] the enhanced $^3J_{C1,C6}$ values observed in *β*-pyranoses can be attributed mainly to the O1 in-plane factor.

Studies of $^3J_{C1,C6}$ values in α- (**4**) and *β*- (**5**) D-galactopyranoses and α- (**16**) and *β*-(**17**) L-fucopyranoses (6-deoxy-L-

(48) Bock, K.; Duus, J. O. *J. Carbohydr. Chem.* **1994**, *13*, 513−543.

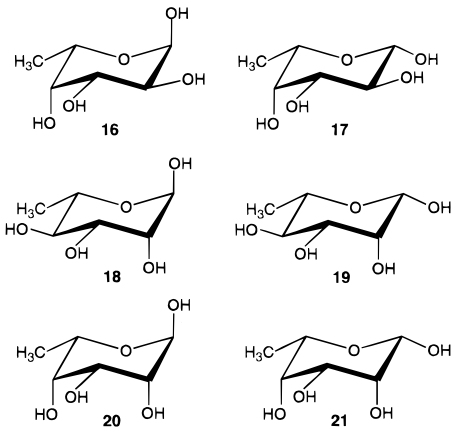

galactopyranoses) (Table 2) show similar differences in couplings *between anomers* (0.9 Hz for *galacto*, 1.2 Hz for *fuco*), again suggesting that O1 is more important than O6 in affecting the *relative* magnitudes of $^3J_{C1,C6}$. Couplings, however, in the fucopyranoses are *smaller* than those observed in the galactopyranoses. Other corresponding J_{CC} values involving C1, however, are similar in *galacto* and *fuco* anomers (Table 2), and thus, the observed differences in $^3J_{C1,C6}$ values cannot be attributed to significant differences in ring conformation. Importantly, comparisons of $^3J_{C1,C6}$ values in mannopyranoses (**10**, **11**) and talopyranoses (**12**, **13**) and their 6-deoxy derivatives (**18**, **19** and **20**, **21**, respectively) (Tables 1 and 2) also show similar differences *between anomers* in the 6-oxy and corresponding 6-deoxy compounds, but, importantly, *the reduction in $^3J_{C1,C6}$ caused by the removal of O6 is not uniformly observed.*

A comparison of $^3J_{C1,C6}$ values in α- and β-D-[6-^{13}C]-glucopyranoses (**6**, **7**) and 6-deoxy-α- and β-D-[6-^{13}C]glucopyranoses (**22**, **23**) (Table 3) shows that, as observed in **4**/**5** and **16**/**17**, $^3J_{C1,C6}$ is smaller in the α-anomers. The slightly larger values of $^3J_{C1,C6}$ in *galacto* isomers (relative to those in *gluco* isomers) may be caused by the slightly larger population of *tg* rotamers found in this ring configuration due to the axial O4.[48] Interestingly, $^3J_{C1,C6}$ values in **6** and **22** and in **7** and **23** are *essentially the same*; this comparison differs from those made between **4** and **16** and between **5** and **17** (see above). The lower percentage of the *tg* rotamer expected in *gluco* isomers (compared to that in *galacto* isomers) is responsible for the similar $^3J_{C1,C6}$ values in **6** and **22** and in **7** and **23**; since the loss of O6 causes a minimal change in $^3J_{C1,C6}$ magnitude, O6 must make a minimal contribution to the observed coupling in *gg* and *gt* conformations. The axial O4 found in galacto- and talopyranoses results in a larger *tg* population in these configurations, and therefore, the loss of O6 causes a *larger decrease* in $^3J_{C1,C6}$ than is observed between gluco- and mannopyranoses and their 6-deoxy derivatives. Thus, the contribution that O6 makes to $^3J_{C1,C6}$ magnitude depends on conformation about the C5−C6 bond, with the in-plane orientation (*tg*) increasing the coupling. Out-of-plane orientations (*gg* and *gt*) exert little effect on $^3J_{C1,C6}$ to the extent that, *when in these conformations, a CH_2OH group is equivalent to a CH_3 group with respect to its influence on $^3J_{C1,C6}$.*

Similar electronegative substituent effects, which range from 1.8 to 4.4 Hz for C3−C4−C5−C6 dihedral angles near 180° (Table 1), also affect $^3J_{C3,C6}$ in D-aldohexopyranoses. As observed for $^3J_{C1,C6}$, an in-plane orientation of the terminal O3 makes a positive contribution to the observed coupling, but other factors are at work. For example, significant differences in $^3J_{C3,C6}$ are observed between *allo* (**2**, **3**) and *gulo* (**8**, **9**) anomers, suggesting that configuration at C4 affects coupling magnitude; this effect may be caused, in part, by changes in hydroxymethyl conformation induced by the orientation of O4 (axial orientation enhances the population of *tg* rotamer).

Table 3. J_{CC} Values[a] in D-[6-^{13}C]Glucopyranoses and 6-Deoxy-D-[6-^{13}C]Glucopyranoses

aldopyranose	$^1J_{C6,C5}$	$^2J_{C6,C4}$	$^3J_{C6,C3}$	$^3J_{C6,C1}$
α-D-*gluco* **6**	43.6	nc	3.9	3.3
6-deoxy-α-D-*gluco* **22**	41.2	nc	3.4	3.4
β-D-*gluco* **7**	43.0	nc	4.4	4.2
6-deoxy-β-D-*gluco* **23**	40.9	nc	3.9	4.1

[a] In Hz, ±0.1 Hz; ^2H_2O solvent, ~21 °C; nc = no coupling observed (J < 0.5 Hz). Data for **6** and **7** were taken from ref 20. No coupling was observed between C1 and C4 in all of the compounds.

It is interesting to note that $^3J_{C1,C6}$ values in **6**/**22** and **7**/**23** are virtually identical; however, significant differences are observed in $^3J_{C3,C6}$ values (Table 3). The similar $^3J_{C1,C6}$ values are attributed to the very small population of *tg* rotamer observed in *gluco* isomers.[48] In contrast, the *gt* rotamer, which orients O6 in the C3−C4−C5−C6 coupling plane, is significantly populated in *gluco* isomers, and thus, the removal of O6 results in a significant reduction (~−0.5 Hz) in $^3J_{C3,C6}$.

Electronegative substituent effects on $^3J_{C1,C6}$ were examined at more remote sites in several deoxyaldopyranoses (Table 2). Couplings in **24** and **25** are virtually identical to those observed in **6** and **7**, respectively (Table 1), indicating that deoxygenation at C2 exerts essentially no effect on $^3J_{C1,C6}$ magnitude. In contrast, $^3J_{C1,C6}$ values in **26**−**29** (Table 2) are considerably *smaller* than those observed in the corresponding 3-oxy compounds by 0.3−0.8 Hz (Table 1). Thus, deoxygenation at C3 appears to influence $^3J_{C1,C6}$; this effect appears related to the anomalous $^3J_{C1,C6}$ values observed in the allopyranoses (**2**/**3**, see above) and may be a through-space phenomenon.

3. $^3J_{CC}$ Values in Ketohexopyranosyl Rings. Trans-*O*-glycosidic C−O−C−C coupling pathways involving *non-anomeric terminal carbons* (e.g., $^3J_{C2,C1,O,CX}$) (Scheme 2) are approximated by the C1−C2−O6−C6 coupling fragment found in conformationally rigid ketohexopyranoses (Scheme 3), and J_{CC} values were measured in four ring configurations: β-D-*fructo* **30**, α-D-*tagato* **31**, β-D-*tagato* **32**, and α-L-*sorbo* **33**

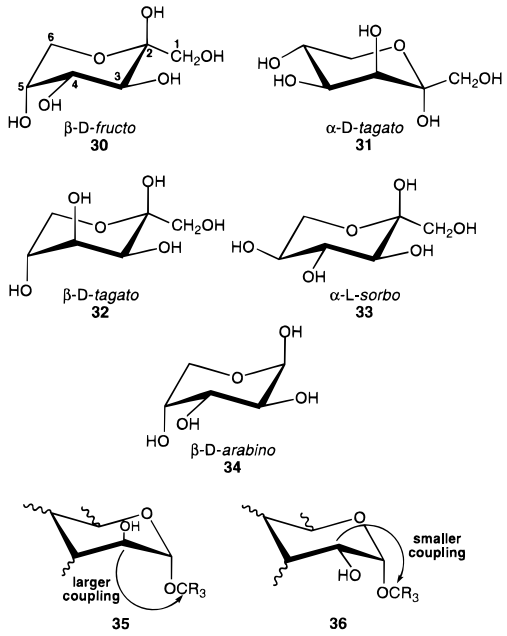

(Table 4).

The preferred ring conformation of **30** is $^2C_5$ in the crystalline state,[49] and this assignment was confirmed in solution by

Table 4. J_{CC} Values[a] for [^{13}C]Ketohexopyranoses **30**−**33** and β-D-[^{13}C]Arabinopyranose **34**

coupled nuclei	β-D-*fructo* **30**	α-D-*tagato* **31**	β-D-*tagato* **32**	α-L-*sorbo* **33**	β-D-*arabino* **34**[b]
C1, C2	49.8	51.0			45.7
C1, C3	2.2	1.7			nc
C1, C4	1.8	1.5			nc[c]
C1, C5					2.1
C1, C6	2.4	3.1	2.0		
C2, C1	49.9	51.0	50.7		
C2, C3	47.4	48.6	46.9		
C2, C4	nc	2.0			
C2, C5[c]	nc	0.8	0.6		
C2, C6	2.1	0.8	nc		
C3, C1	2.5				
C3, C2	47.6				
C3, C4	39.8				
C3, C5	nc				
C3, C6[c]	1.7				
C4, C1				1.9	
C4, C2				nc	
C4, C3				38.3	
C4, C5				38.5	
C4, C6				1.3	
C5, C1					1.9
C5, C2[c]				nc	1.8
C5, C3				3.0	nc
C5, C4				38.8	37.5
C5, C6				39.5	
C6, C1	obs			2.4	
C6, C2	2.1			2.0	
C6, C3[c]	1.4			nc	
C6, C4	nc			1.4	
C6, C5	37.3			39.3	

[a] In Hz, ±0.1 Hz; ^2H_2O solvent, ∼21 °C; nc = no coupling was observed (J < 0.5 Hz). No coupling was observed between C1 and C5 in the *fructo* and *tagato* ring configurations. Obs = obscured signal prevented J coupling measurement. [b] Data taken from refs 20 and 71. [c] Dual-pathway couplings.

comparing J_{CC} values in **30** with corresponding couplings observed in **34**; the latter prefers the $^1C_4$ geometry[20,50] which has the same relative configuration as that found in the $^2C_5$ form of **30**. Corresponding J_{CC} values in **30** and **34** (Table 4) are similar and confirm that **30** prefers the $^2C_5$ form. In this conformation, the dihedral angle between C1 and C6 is ∼180°, and $^3J_{C1,C6}$ = 2.4 Hz.

α-D-Tagatopyranose **31** is expected to prefer the $^5C_2$ conformation in aqueous solution, as observed in the crystalline state.[51] In the $^5C_2$ form of **31**, $^3J_{C1,C6}$ = 3.1 Hz, which corresponds to a C1−C2−O6−C6 dihedral angle near 180°.

β-D-Tagatopyranose **32** probably prefers the $^2C_5$ conformation, but contributions from the alternate $^5C_2$ form are likely. The $^3J_{C1,C6}$ value of 2.0 Hz in **32**, which is smaller than that observed in **30**, supports this contention and compromises the use of **32** as a model compound.

$^3J_{C1,C6}$ values in **30** and **31** span a 2.4−3.1 Hz range for a C1−C2−O6−C6 dihedral angle of ∼180°. This broad range is attributed to different C1−C2 rotamer populations induced by differences in configuration at C3 (Scheme 7). Rotamer C is expected to have similar stability in **30** and **31**; two opposing factors, namely, unfavorable sterics and favorable stereoelectronics, will determine its stability.[52−55] Rotamer B, however, will be destabilized in **30** due to the presence of a 1,3-interaction between O1 and the equatorial O3, and Rotamer A will be destabilized in **31** due to the presence of a 1,3-interaction between O1 and the axial O3. Thus, the larger $^3J_{C1,C6}$ value in **31** relative to that in **30** is attributed to the more predominant Rotamer B in the former *which orients O1 in the C1−C2−O6−C6 coupling plane*. This interpretation is supported by the observed $^3J_{C1,C6}$ value in **33**, which highly prefers the $^2C_5$ conformation[56] and has the same configuration at C2, C3, and C4 as **30**. In **33**, $^3J_{C1,C6}$ = 2.4 Hz (Table 4), which is identical to $^3J_{C1,C6}$ in **30**. Thus, the importance of the orientation of *terminal* electronegative substituent(s) along C−O−C−C coupling pathways is reaffirmed in the ketosugars.

Scheme 7

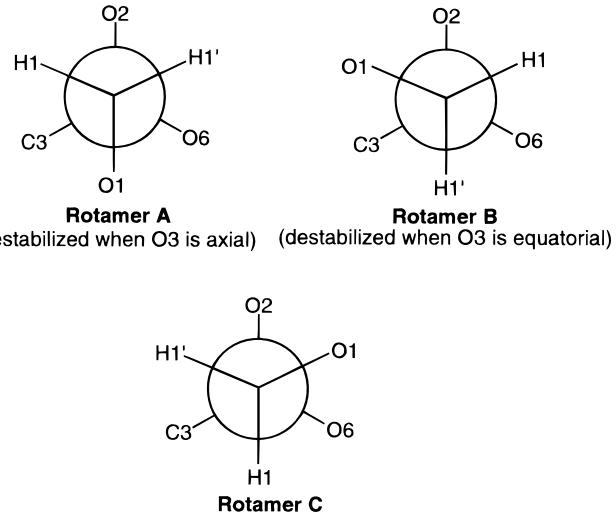

A comparison of $^3J_{C1,C6}$ values observed in **2**−**29** with $^3J_{C1,C6}$ values observed in **30**, **31**, and **33** for C−O−C−C dihedral angles of ∼180° reveals a coupling range of 2.4−4.9 Hz, demonstrating that the C−O−C−C pathway structure, in addition to dihedral angle, plays a major role in dictating coupling magnitude. In addition, the C1−C2−O6−C6 coupling pathway in **30**, **31**, and **33** yields couplings that are, on average, smaller than those observed for the C1−O5−C5−C6 pathway in **2**−**29**, suggesting that the AO21 and 1AO1 pathways may not obey the same Karplus relationship. Furthermore, in the context of *O*-glycoside linkage analysis, the orientation of terminal electronegative substituents on both pathways can be important. For example, $^3J_{C2,C1,O,CX}$ values involving α-D-aldopyranosyl rings having an axial O2 (e.g., **35**) should display larger couplings than those having an equatorial O2 (e.g., **36**) for the same dihedral angle, since O2 lies in the coupling plane in the former but not in the latter.

4. $^2J_{CC}$ and $^3J_{CC}$ Values in Hindered Glycosides. Ethyl and isopropyl D-gluco- and D-mannopyranosides **37**−**44** were prepared with ^{13}C-enrichment at C1 or C2 to examine the trans-*O*-glycosidic couplings involving C1 and C2 (Table 5) and to evaluate the effect, which was predicted above (see **35** and **36**), of C2 configuration on C2−C1−O1−CX couplings. The aglycone groups of **37**−**44** are larger than those in methyl glycosides, and thus, rotation about the C1−O1 bond is expected to be more hindered.

The $^2J_{C1,CH/CH_2}$ values observed in **37**−**44** (−1.8 ± 0.1 Hz, Table 5) are negative in sign[8] and are independent of aglycone structure (ethyl, isopropyl), configuration at C1 (α, β), and

(49) Kanters, J. A.; Roelofsen, G.; Alblas, B. P.; Meinders, I. *Acta Crystallogr.* **1977**, *B33*, 665- 672.
(50) Bock, K.; Pedersen, C. *Acta Chem. Scand.* **1975**, *B29*, 258−264.
(51) Takagi, S.; Rosenstein, R. D. *Carbohydr. Res.* **1969**, *11*, 156−158.
(52) Wolfe, S. *Acc. Chem. Res.* **1972**, *5*, 102−111.
(53) Zefirov, N. S.; Samoshin, V. V.; Subbotin, O. A.; Baranenkov, V. I.; Wolfe, S. *Tetrahedron* **1978**, *34*, 2953−2959.
(54) Kirby, A. J. *The Anomeric Effect and Related Stereoelectronic Effects at Oxygen*; Springer: New York, 1983.
(55) Wiberg, K. B.; Murcko, M. A.; Laidig, K. E.; MacDougall, P. J. *J. Phys. Chem.* **1990**, *94*, 4, 6956−6959.
(56) Kim, S. H.; Rosenstein, R. D. *Acta Crystallogr.* **1967**, *22*, 648−656.

Table 5. J_{CC} Values[a] in Ethyl and Isopropyl Gluco- and Mannopyranosides

	ethyl[c]				isopropyl[c]			
coupled nuclei	αG (**37**)	βG (**38**)	αM (**41**)	βM (**42**)	αG (**39**)	βG (**40**)	αM (**43**)	βM (**44**)
C1, C2	46.7	46.9	47.2	43.8	46.7	46.9	47.2	44.0
C1, C3[d]	nc	4.5	nc	3.9	nc	4.7	nc	4.1
C1, C5[e]	2.0	nc	2.0	nc	2.0	nc	2.1	nc
C1, CH/CH_2[e]	1.8	1.8	1.8	1.8	1.7	1.8	1.7	1.7
C1, C4	nc	nc	0.7[f]	nc	nc	nc	0.8[f]	nc
C1, C6	3.3	4.1	3.2	4.0	3.3	4.1	3.2	4.1
C1, CH_3	2.8	2.8	2.8	3.0	2.0	2.1	2.1	2.1
C1, CH_3' [b]					1.4	1.6	1.1	1.4
C2, C1	46.7	46.9	47.2	43.8	46.7	46.9	47.4	44.0
C2, C3	38.2	38.9	37.8	38.2	38.2	39.0	obsc	38.2
C2, C4[d]	3.0	2.7	nc	0.3[f]	3.0	2.7	nc	nc
C2, C5	nc	nc	nc	nc	nc	nc	nc	nc
C2, CH/CH_2	2.7	3.0	3.4	2.8	2.7	~3.0	3.1	2.5

[a] In Hz, ^2H_2O solvent, 30 °C; nc = no coupling was observed (J < 0.5 Hz). [b] More-shielded methyl signal. [c] αG = α-*gluco*; βG = β-*gluco*; αM = α-*manno*; βM = β-*manno*. [d] Coupling signs are probably positive. [e] Coupling signs are probably negative.[8a] [f] Coupling sign uncertain.

configuration at C2 (*gluco*, *manno*). On the basis of recent reports,[8] these couplings are expected to be relatively insensitive to psi (ψ), but sensitive to phi (ϕ). Their magnitudes suggest that Rotamer II (Scheme 8) cannot be a major contributor in solution since $^2J_{COC}$ is expected to be very small or zero in this rotamer. Thus, Rotamers I and III are possible contributors, but in α-anomers, Rotamer I should become less stable as the aglycone increases in size. The $^2J_{C1,CH/CH_2}$ values observed in **37**, **39**, **41**, and **43** can, therefore, be correlated with Rotamer III, which is also favored based on stereoelectronic considerations (competing endo- and exoanomeric effects[57]). The distinction between Rotamers I and III is less clear for β-anomers since steric constraints appear less demanding for Rotamer I than those in α-anomers. However, $^3J_{CH}$ values of 4.6 Hz have been observed between the aglycone carbon and H1 in methyl, ethyl, and isopropyl β-D-glucopyranosides, and these and other experimental and computational results indicate that Rotamer III is highly favored in solution.[58] In addition, previous arguments suggest that the exoanomeric effect, which favors Rotamer III, should be stronger in β-anomers than in α-anomers.[57c] It should be noted, however, that Rotamer I will be destabilized in β-mannopyranosides (relative to β-glucopyranosides) by the presence of a 1,3-interaction between the aglycone carbon and the axial O2 (a similar destabilization exists in Rotamer II for β-glucopyranosides), and this observation in combination with the factors discussed above leads to the conclusion that, at least for **42** and **44**, Rotamer III should be highly favored in solution.

The above C1−O1 torsional constraints based on $^2J_{COC}$ analysis and structural considerations lead to an interpretation of $^3J_{COCC}$ values across the glycosidic linkages of **37**−**44**. Coupling between C2 and the aglycone carbon ($^3J_{C2,CH/CH_2}$) (Table 5) depends, in part, on the ϕ torsion angle (Scheme 1). In the α-glycosides, this coupling varies from 2.7 to 3.4 Hz, and corresponds to C2−C1−O−CH/CH_2 dihedral angles of ~180°; these values are similar to $^3J_{C1,C6}$ values observed in ketohexopyranoses **30**, **31**, and **33** (2.4−3.1 Hz, Table 4) in a pathway where, like $^3J_{C2,CH/CH_2}$ in **37**−**44**, only one of the *coupled* carbons bears an electronegative hydroxyl group. Couplings in **37** and **39** are identical, indicating that the additional alkyl group on the aglycone carbon does not affect coupling appreciably; a small difference, however, is observed between **41** and **43**, which may be due in part to a small difference in the C1−O1 torsion angles. It should be noted that $^3J_{C2,CH/CH_2}$ in α-*gluco* isomers **37** and **39** is *smaller* (2.7 Hz) than that observed in α-*manno* isomers **41** and **43** (3.3 ± 0.2 Hz) despite similar dihedral angles, and this difference is attributed to the in-plane effect of the axial O2 in α-*manno* isomers, which is expected to enhance coupling as predicted above (e.g., **35**, **36**). The difference, ~0.6 Hz, is similar in magnitude to the average difference observed in $^3J_{C1,C6}$ values between α- and β-D-aldohexopyranoses (0.6 Hz, Table 1), and between **30**/**33** and **31** (0.7 Hz, Table 4).

$^3J_{C2,CH/CH_2}$ values in the β-anomers **38**, **40**, and **42** (2.9 ± 0.1 Hz, Table 5) are similar to those observed in the α-anomers, suggesting that ϕ is not notably different in the two anomeric configurations. The smallest coupling is found in **44** and may indicate a small change in C1−O1 torsion angle.

The preceding analysis of $^2J_{COC}$ and $^3J_{C2,CH/CH_2}$ values in **37**−**44** is internally consistent and indicates a strong preference for Rotamer III about the C1−O1 bond (ϕ) in these compounds. This constraint permits a treatment of the trans-*O*-glycosidic $^3J_{COCC}$ values in **37**−**44** involving C1. These couplings are sensitive to the O1−CH/CH_2 torsion angle, which is denoted as ψ (Scheme 1). Couplings between C1 and CH_3 in the ethyl glycosides **37**−**38** and **41**−**42** are 2.9 ± 0.1 Hz (Table 5). This coupling pathway is similar to the C1−O5−C5−C6 pathway in **16**, **18**, **20**, and **22** where the terminal O1 does not lie in the coupling plane; $^3J_{C1,C6}$ in these compounds is 3.2 ± 0.2 Hz (Tables 2 and 3). These results indicate that the C1−O1−CH_2−CH_3 dihedral angle in **37**−**38** and **41**−**42** favors a trans orientation, although some contribution from gauche conformations probably occurs.

5. Estimations of $^3J_{COCC}$ for Gauche Conformations. Methyl 3,6-anhydro-α-D-[1-^{13}C]glucopyranoside **47** contains a

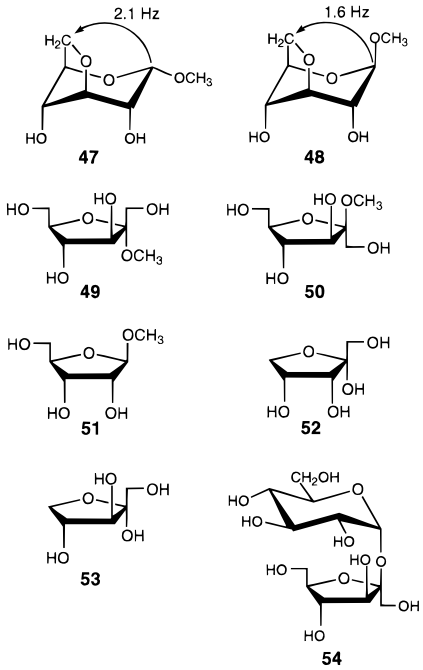

C1−O5−C5−C6 coupling pathway with a dihedral angle of ~45°.[59,60] In **47**, $^3J_{C1,C6}$ = 2.1 Hz (Table 6). In methyl 3,6-anhydro-β-D-[1-^{13}C]glucopyranoside **48**, which contains a similar coupling pathway, $^3J_{C1,C6}$ = 1.6 Hz (Table 6). The larger

(57) (a) Lemieux, R. U.; *Pure Appl. Chem.* **1971**, *25*, 527−548. (b) Lemieux, R. U.; Koto, S.; Voisin, D. In *Anomeric Effect: Origin and Consequences*; Szarek, W. A., Horton, D., Eds.; ACS Symposium Series 87; American Chemical Society: Washington, DC, 1979; pp 17−29. (c) Praly, J.-P.; Lemieux, R. U. *Can. J. Chem.* **1987**, *65*, 213−223.

(58) Lemieux, R. U.; Koto, S. *Tetrahedron* **1974**, *30*, 1933−1944.

Scheme 8

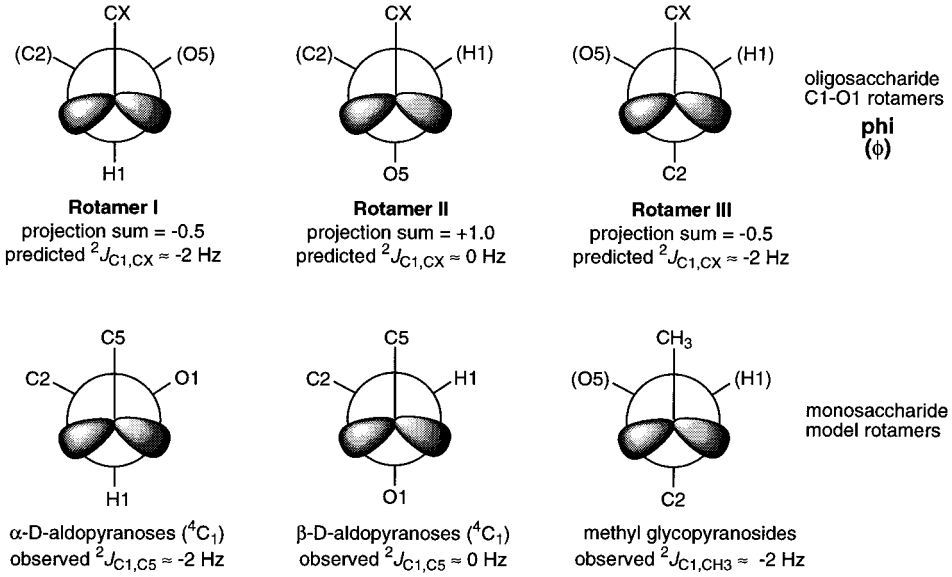

Table 6. J_{CC} Values and ^{13}C Chemical Shifts in Methyl 3,6-Anhydro-α-D-[1-^{13}C]Glucopyranoside **47** and Methyl 3,6-Anhydro-β-D-[1-^{13}C]Glucopyranoside **48**

	coupling constants (Hz)					
compd[a]	$^1J_{C1,C2}$	$^2J_{C1,C3}$	$^{3+3}J_{C1,C4}$	$^2J_{C1,C5}$	$^3J_{C1,C6}$	$^2J_{C1,OCH_3}$
3,6-anhydro-α- (**47**)	43.1	1.9[b]	0.8[b]	1.4[b]	2.1	1.9
3,6-anhydro-β- (**48**)	46.3	1.3[b]	0.9[b]	2.4[b]	1.6	2.0

	chemical shifts (ppm)[b]						
	C1	C2	C3	C4	C5	C6	CH_3
3,6-anhydro-α- (**47**)	99.9	70.7	72.2	72.4	76.8	70.2	58.8
3,6-anhydro-β- (**48**)	104.4	73.1	72.9	72.2	75.7	70.6	56.9

[a] ^2H_2O solvent, ~21 °C. [b] Signal assignments for **47** and **48** were modified from those reported in ref 75; the C6 assignments were confirmed by APT and the C2 assignments were reassigned through observation of the large $^1J_{CC}$ splitting. The signal assignments for C3−C5 in **47** and **48** and the corresponding J_{CC} values associated with these carbons, require experimental verification.

coupling observed in **47** (Δ = 0.5 Hz) is caused by the O1 "in-plane" effect, which occurs for C−O−C−C dihedral angles of ~60° as well as ~180° (see above).

Additional information on $^3J_{COCC}$ values for 60° dihedral angles is derived from studies of methyl α- (**49**) and β- (**50**) D-fructofuranosides.[5] $^2J_{C2,OCH_3}$ values in **49** and **50** are 2.3 and 2.4 Hz, respectively (probably negative in sign[8]), and suggest that the C2−O2 conformation orienting CH_3 anti to O5 is a minor rotamer in solution.[8] Of the two remaining C2−O2 conformers, that orienting CH_3 gauche to O5 and C1 (θ = ~60°) is expected to be more favored due to the exoanomeric effect.[57] $^3J_{C1,CH_3}$ values are 1.8 and 2.3 Hz in **49** and **50**, respectively, which are similar to the $^3J_{C1,C6}$ values observed in **47** and **48**. $^3J_{C3,OCH_3}$ values of 2.4 and 1.8 Hz are observed in **49** and **50**, respectively, and these couplings would be correlated with an anti (or near anti) arrangement of C3 and CH_3 if the above structural arguments are valid. These values, however, appear small and may indicate that some contribution from the C2−O2 rotamer having C1 anti to CH_3 may exist, especially in **49**, but these couplings need to be compared to related values in other ketoglycosides before a firm interpretation is possible. Interestingly, however, $^3J_{C3,CH_3}$ is larger in **49** than in **50**; in the preferred ring conformation of **49** (near E_2),[5] O3 lies in the C3−C2−O2−CH_3 coupling plane, and thus, the enhanced coupling may be due to this in-plane effect as well as to differences in the C2−O2 torsions.

6. J_{COCC} Values in Conformationally Flexible Compounds. In some cases, correlations between $^3J_{COCC}$ and dihedral angle can be made with reasonable confidence in conformationally flexible molecules if sufficient data on their solution behaviors are available. It should be understood, however, that the coupling−dihedral angle correlations derived from flexible molecules are subject to larger uncertainties than those derived from rigid molecules.

Methyl β-D-Ribofuranoside (51). $^3J_{C1,C5}$ has been estimated to be ~0.5 Hz in [1-^{13}C]**51**,[25] and an analysis of $^3J_{HH}$ data using the PSEUROT program[61] indicated that two nonplanar forms are preferred in aqueous solution, namely, E_2 (~90%) and ^2E (~10%).[62] *Ab initio* molecular orbital calculations on both forms[62] gave C1−O4−C4−C5 dihedral angles of ~123°.

An analysis of the dual-pathway coupling, $^{2+3}J_{C1,C3}$, in **51** provides an *estimation* of the $^3J_{COCC}$ value associated with a dihedral angle of ~0°. The observed coupling is expected to be the algebraic sum of the constituent two-bond (C1−C2−C3) and three-bond (C1−O4−C4−C3) pathways.[10] Coupling along the two-bond pathway should be similar in the preferred E_2 and ^2E forms (since the *terminal* hydroxyl groups at C1 and C3, which are key determinants of $^2J_{CCC}$ magnitude and sign,[8a,20] assume the same relative orientation in both ring conformations[63]) and is expected to be small or zero. $^{2+3}J_{C1,C3}$ in **51** is (+)3.0 Hz, leading to the conclusion that the $^3J_{C1,C3}$ component is primarily responsible for the observed coupling. In E_2 and ^2E, the C1−O4−C4−C3 torsion angle is ~0°.

α-D-*Erythro*- (52) and α-D-*Threo*-(53) 2-Pentulofuranoses. Recent analyses[35] of J_{HH} and J_{CH} values in **52** and **53** indicate

(59) Campbell, J. W.; Harding, M. M. *J. Chem. Soc., Perkin Trans. 2* **1972**, 1721−1723.

(60) Reference 59 reports the crystal structure of methyl 3,6-anhydro-α-D-galactopyranoside; we assume that the C1−C6 dihedral angle in this compound is similar to those in **47** and **48**, the crystal structures of which have not been determined.

(61) PSEUROT 6.2, Gorlaeus Laboratories, University of Leiden.

(62) Podlasek, C. A.; Stripe, W. A.; Carmichael, I.; Shang, M.; Basu, B.; Serianni, A. S. *J. Am. Chem. Soc.* **1996**, *118*, 1413−1425.

(63) Bandyopadhyay, T.; Wu, J.; Stripe, W. A.; Carmichael, I.; Serianni, A. S. *J. Am. Chem. Soc.* **1997**, *119*, 1737−1744.

that both compounds prefer conformations near $E_2/^3E$ in which the C1−C2−O5−C5 dihedral angle is ∼154°. The observed $^3J_{C1,C5}$ in **52** and **53** is 2.0 Hz.[35]

Methyl α- (49) and *β*- (50) D-Fructofuranosides and Sucrose 54. Analyses of J_{HH} and J_{CH} values in **49** and **50** have shown that they prefer "south" (E_2) and "north" (^2E) conformations, respectively,[5] and the C1−C2−O5−C5 torsion angles in these conformations are ∼164° and ∼156°, respectively. $^3J_{C1,C5}$ in **49** = 2.7 Hz, and $^3J_{C1,C5}$ in **50** = 1.9 Hz.[5] In addition, $^3J_{C2,C6}$ values are 2.3 Hz and <0.8 Hz in **49** and **50**, respectively, and these couplings correlate with C2−O5−C5−C6 torsion angles of ∼150° and ∼102°, respectively. In sucrose **54,** the preferred conformation of the *β*-D-fructofuranosyl ring is near $^4T_3$, as determined by NMR[5] and X-ray crystallography.[64] In this geometry, the C1−C2−O5−C5 and C2−O5−C5−C6 dihedral angles are ∼133°, and $^3J_{C1,C5}$ and $^3J_{C2,C6}$ values in **54** are both < 0.8 Hz.[5]

7. Theoretical Calculations of J_{CC} Values in Model Systems. We demonstrated previously that trends in computed J_{CH} and J_{CC} values in *β*-D-ribofuranose[62] and 2-deoxy-*β*-D-*erythro*-pentofuranose[65] could be predicted reliably using *ab initio* molecular orbital methods even at the HF level. Accurate assessment of the *magnitude* of these coupling constants, however, requires consideration of the effects of electron correlation. In previous work,[8a,62,65,66] correlation effects were introduced either approximately by second-order Møller−Plesset perturbation theory (MP2) or more completely by quadratic configuration interaction (QCISD).[36,67] A range of scaling factors was developed[66,67] enabling a reduction in the MP2 corrections to the more quantitative QCISD values in systems which are prohibitively large for calculation at the latter level. Alternatively, such correlation corrections may be derived from density functional theory (DFT)[68] at a computational cost not much greater than that of HF calculations. This treatment is capable of providing reliable magnitudes for $^{13}C-^{13}C$, $^{13}C-^1H$ and $^1H-^1H$ spin-couplings in a wide range of bonding environments and provides a near quantitative description of the various couplings in a 2-deoxyribofuranosyl ring.[69] Consequently, the DFT approach was adopted to calculate spin-couplings in the model systems discussed below.

A. Model System 1. The computational method was first validated by examining model structures **55** and **56** where computed couplings can be compared to experimental data. $^2J_{C1,C3}$, $^2J_{C1,C5}$, and $^3J_{C1,C6}$ values were calculated in each structure for three rotamers about the C5−C6 bond (*gt, gg, tg*; Scheme 6). In all of the calculations, the initial C1−O1 torsion was chosen to orient OH1 gauche to O5 and H1, which is expected to be preferred on the basis of stereoelectronic considerations,[57,58] and the initial C6−O6 torsion was chosen arbitrarily to orient OH6 anti to C5. The six initial structures converged smoothly to yield energetically stable geometries (see Scheme 1 in Supporting Information for structural models of the optimized geometries), and computed couplings are found in Table 7 (structural parameters and conformational energies for **55** and **56** are found in Table 1 of Supporting Information).

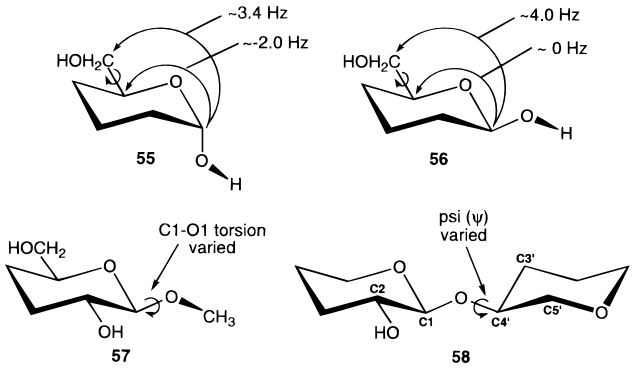

Calculated $^2J_{C1,C5}$ values are ∼ −2.2 Hz and ∼ −1.0 Hz when O1 is axial (**55**) and equatorial (**56**), respectively, and are consistent with the ∼−2.0 Hz couplings observed in α-pyranoses and the small or zero couplings observed in *β*-pyranoses.[8a,71,72] Calculated $^2J_{C1,C3}$ values in **55** are considerably more negative than those in **56**. Projection resultants for the C1−C2−C3 coupling pathways in **55** and **56** are −1.0 and +0.5, respectively, yielding predicted couplings of ∼−3.0 Hz and ∼0 Hz, respectively, in good agreement with the computed values.

Computed $^3J_{C1,C6}$ values in **55** and **56** confirm the structure-coupling correlations discussed above on the basis of experimental data. In each C5−C6 rotamer, the $^3J_{C1,C6}$ value is larger in **56** than in **55**. The computed difference (∼0.6 Hz) is similar to that observed experimentally and confirms that $^3J_{C1,C6}$ is enhanced when O1 lies in the C1−O5−C5−C6 coupling plane. Furthermore, the $^3J_{C1,C6}$ magnitude depends on the C5−C6 bond conformation. Computed couplings in the *tg* rotamers (where O6 lies in the C1−O5−C5−C6 coupling plane) (Scheme 6) are larger (Δ = 1.0−1.4 Hz) than couplings in *gg* and *gt* rotamers. Smaller differences in $^3J_{C1,C6}$ are observed between *gg* and *gt* rotamers (<0.4 Hz).

Overall, the computed couplings in **55** and **56** are in satisfactory agreement with experimental data with respect to their magnitudes and correlations with molecular structure, thus justifying an extension to systems less accessible by experiment.

B. Model System 2. Model compound **57** was studied as a function of the C1−O1 bond torsions defined in Scheme 9. Calculations were performed with O6 gauche to O5 and H5 (*gt* rotamer; Scheme 6), OH6 anti to C5, and OH2 anti to C1. Fully optimized geometries were obtained for the *g′g′* and *g′t′* rotamers (Scheme 9); the optimized O5−C1−O1−CH_3 torsion angles were 66.4 and −68.9°, respectively. Full geometry optimization was not possible for the *t′g′* rotamer since rotation about the C1−O1 bond to give the *g′t′* rotamer occurred spontaneously during optimization. Therefore, the H1−C1−O1−CH_3 torsion angle was fixed at −60°. Computed couplings for **57** are given in Table 8 (relevant structural parameters and conformational energies are given in Table 2 of Supporting Information).

Computed $^2J_{C1,C3}$ values in **57** range from 0.6 to 1.4 Hz, and the calculated projection resultant (+1.5) yields a predicted coupling of ∼+2 Hz. These computed couplings were compared to $^2J_{C1,C3}$ values in **26**−**29** (Table 2). $^2J_{C1,C3}$ values in **26** and **27** are −2.0 and +1.0 Hz, respectively, and the latter value is in close agreement with the computed $^2J_{C1,C3}$ value in

(64) (a) Hanson, J. C.; Sieker, L. C.; Jensen, J. H. *Acta Crystallogr. Sect. B* **1973**, *29*, 797−808. (b) Brown, G. M.; Levy, H. A. *Acta Crystallogr. Sect. B* **1973**, *29*, 790−797.

(65) Church, T. J.; Carmichael, I.; Serianni, A. S. *J. Am. Chem. Soc.* **1997**, *119*, 8946−8964.

(66) Serianni, A. S.; Wu, J.; Carmichael, I. *J. Am. Chem. Soc.* **1995**, *117*, 8645−50.

(67) Carmichael, I.; Chipman, D. M.; Podlasek, C. A.; Serianni, A. S. *J. Am. Chem. Soc.* **1993**, *115*, 10863−70.

(68) Malkin, V. G.; Malkina, O. L.; Eriksson, L. A.; Salahub, D. R. in *Modern Density Functional Theory: A Tool for Chemistry*; Seminario, J. M., Politzer, P., Eds.; Elsevier Science B. V., 1995; Vol. 2, pp 273−347.

(69) Cloran, F.; Carmichael, I.; Serianni, A. S. *J. Am. Chem. Soc.*, submitted for publication.

(70) Walker, T. E.; London, R. E.; Whaley, T. W.; Barker, R.; Matwiyoff, N. A. *J. Am. Chem. Soc.* **1976**, *98*, 5807−5813.

(71) King-Morris, M. J.; Serianni, A. S. *J. Am. Chem. Soc.* **1987**, *109*, 3501−3508.

(72) Barker, R.; Walker, T. E. *Methods Carbohydr. Chem.* **1980**, *8*, 151−165.

Table 7. Computed J_{CC} Values[a] in Model Compounds **55** and **56**

compd[b]	$^2J_{C1,C3}$	$^2J_{C1,C5}$	$^3J_{C1,C6}$
55 (*gg*)[c]	−2.7	−2.3	3.6 (−178.4°)[d]
55 (*gt*)	−2.7	−2.2	3.4 (−178.1°)
55 (*tg*)	−2.7	−2.1	4.7 (−179.4°)
56 (*gg*)	−0.1	−1.1	4.3 (−174.5°)
56 (*gt*)	−0.1	−1.1	3.9 (−175.0°)
56 (*tg*)	−0.2	−0.9	5.3 (−175.5°)

[a] In Hz. [b] In all calculations, the C1−O1 torsion was optimized with the hydroxyl proton *gauche* to H1 and O5, and the C6−O6 torsion was optimized with the hydroxyl proton *anti* to C5. [c] Symbols in parenthesis denote hydroxymethyl conformation (Scheme 6). [d] Data in parentheses are the C1−O5−C5−C6 torsion angles observed in the geometrically optimized structures.

Scheme 9

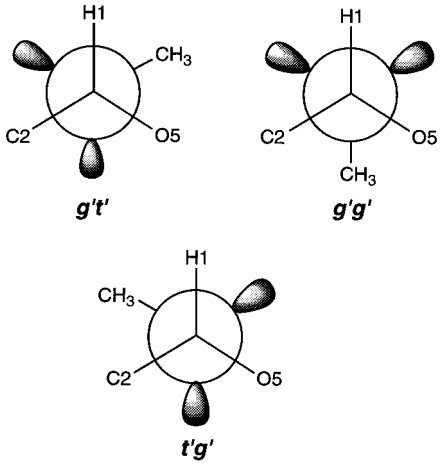

Table 8. Computed J_{CC} Values[a] in Model Compound **57**

C1−O1 rotamer[b]	$^2J_{C1,C3}$	$^2J_{C1,C5}$	$^3J_{C1,C6}$	$^2J_{C1,CH_3}$	$^3J_{C2,CH_3}$
*g′*g′	1.4	−1.0	4.1 (−174.5°)	−2.8	3.2 (−56.0°)
g′t′	1.4	−1.2	4.0 (−173.4°)	−2.2	4.4 (171.6°)
*t′*g′ [c]	0.6	−0.5	4.4 (−172.9°)	0	0 (60°, fixed)

[a] In Hz. [b] Rotamer symbolism is defined in Scheme 9; values in parentheses are the relevant torsion angles determined in the geometrically-optimized structure (see text). [c] The H1−C1−O1−CH_3 torsion angle was fixed at −60° in this calculation.

57, as expected, since **57** and **27** have related structures. Identical projection resultants (+1.5) are calculated for **27** and **29**, and indeed, similar $^2J_{C1,C3}$ values are observed in these structures (Table 2). Likewise, similar resultants are calculated for **26** and **28** (0), leading to a predicted value of ∼−2.0 Hz for $^2J_{C1,C3}$; couplings of 1.8 and 2.0 Hz are observed, and presumably, these are negative in sign.

Computed $^2J_{C1,C5}$ values range from −0.5 to −1.0 Hz and are consistent with the small or zero $^2J_{C1,C5}$ values observed in β-pyranoses (Table 5). Interestingly, the $^2J_{C1,C5}$ value in **27** (and **29**) is larger than expected on the basis of observations in compounds such as **38** and **42**, in agreement with calculations and suggesting that structure at C3 may affect this coupling in aldopyranosyl rings.

$^3J_{C1,C6}$ values range from 4.0 to 4.4 Hz, again consistent with experimental $^3J_{C1,C6}$ values in β-aldohexopyranoses (Table 1), but larger than the $^3J_{C1,C6}$ value observed in **27** (Table 2). The latter difference may reflect, in part, different hydroxymethyl rotamer populations in solutions of **27** than exist for the fully hydroxylated aldohexopyranoses. These data also indicate that rotation about the C1−O1 bond does not significantly affect $^3J_{C1,C6}$ values, and thus lone-pair effects (Scheme 5) on $^3J_{CC}$ do not appear to be important.

Scheme 10

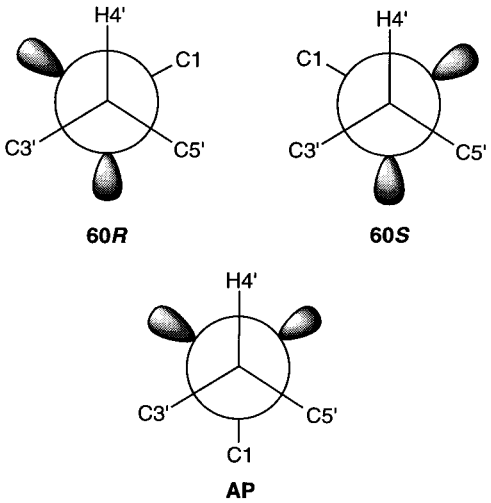

Table 9. Computed J_{CH} and J_{CC} Values[a] in the Model Disaccharide **58**

coupling constant	60*R*[b]	60*S*	AP
$^3J_{C1,H4'}$	5.6 (21.7°)[c]	5.8 (−17.1°)	7.9 (170.7°)
$^3J_{C4',H1}$	4.0 (43.4°)	4.1 (47.5°)	4.3 (31.9°)
$^2J_{C1,C4'}$	−1.9	−2.0	−2.4
$^3J_{C1,C3'}$	2.4 (141.3°)	−0.1 (104.5°)	0.5 (−72.3°)
$^3J_{C1,C5'}$	−0.1 (−98.5°)	3.7 (−134.9°)	1.9 (55.0°)
$^3J_{C2,C4'}$	3.8 (163.8°)	4.2 (167.8°)	3.7 (152.0°)

[a] In Hz. [b] Conformations about psi (ψ) are defined in Scheme 10. [c] Values in parentheses are torsion angles determined in the geometrically-optimized structures (see text).

$^2J_{C1,CH_3}$ values range from 0 to −2.8 Hz, with a zero coupling calculated in the *t′g′* rotamer and considerably more negative couplings (−2.2 and −2.8 Hz) calculated in the *g′g′* and *g′t′* forms. These results are consistent with previous predictions of $^2J_{COC}$ behavior; the *t′*g′ rotamer was predicted to exhibit a zero coupling, and the *g′g′* and *g′t′* rotamers couplings of ∼−2 Hz (Scheme 8).[8a]

The $^3J_{C2,CH_3}$ value for the *g′t′* rotamer is 4.4 Hz and corresponds to the geometry having C2 and CH_3 anti. Interestingly, the gauche geometries, *g′g′* and *t′g′*, yield considerably different couplings, perhaps due to differences in the C2−C1−O1−CH_3 torsion angles (Table 8) and effects caused by fixing the C1−O1 torsion in the *t′g′* rotamer. This observation deserves further scrutiny.

C. Model System 3. The disaccharide model **58** was studied as a function of the glycosidic torsion angle, psi (ψ). A single initial set of exocyclic bond torsions was chosen: OH2 anti to C1 and C4′ anti to C2 (ϕ). Both pyranosyl rings assumed the $^4C_1$ conformation. Geometric optimizations starting with each of the three staggered rotamers about ψ (defined as 60*R*, 60*S*, and AP (Scheme 10); see Scheme 2 in Supporting Information for structural models of these optimized geometries) proceeded smoothly, and representative structural parameters (bond lengths, angles, torsions) and conformational energies are given in Table 3 of Supporting Information. Calculations of the trans-*O*-glycosidic $^2J_{COC}$, $^3J_{COCC}$, and $^3J_{COCH}$ values were then conducted in each geometrically optimized structure (Table 9).

Computed values of $^2J_{C1,C4'}$ do not vary significantly with ψ (−1.9 to −2.4 Hz), in agreement with predictions made earlier.[8a] $^3J_{COCH}$ values vary from 4 to 7.9 Hz, and $^3J_{COCC}$ values vary from ∼0 to 4.2 Hz. Given the range of dihedral angles sampled

Table 10. Comparison of Computed J_{CH} and J_{CC} Values[a] in **57** and Corresponding Couplings Observed in Methyl β-D-glucopyranoside **59**

coupling constant	**57**[b]	**59**
$^1J_{C1,H1}$	152.7	161.3
$^2J_{C1,H2}$	−6.1	−6.3
$^3J_{C1,H5}$	2.2	2.3
$^3J_{C1,H3R}$	2.3	1.2
$^3J_{C1,H3S}$	7.8	6.0[c]
$^1J_{C1,C2}$	53.6	46.9

[a] In Hz. [b] Calculations were conducted in the *g′t′* rotamer (Scheme 9). [c] Coupling observed in methyl β-D-allopyranoside.

in **58**, the data in Table 9 can be used to construct theoretical Karplus curves for the C−O−C−H and C−O−C−C coupling pathways across the *O*-glycosidic linkage, provided that the computed couplings can be considered quantitative. The latter problem was addressed by comparing the J_{CH} and J_{CC} values calculated in a similar fashion in the *g′t′* rotamer of **57** with those observed experimentally in methyl β-D-glucopyranoside **59** (Table 10). The observed $^1J_{C1,H1}$ value is ∼5% *larger* than the computed value, in good agreement with similar comparisons made in aldofuranosyl rings.[69] A similar percent difference also appears to apply to the longer-range $^{13}C-^1H$ couplings. In contrast, the observed $^1J_{C1,C2}$ value is ∼14% *smaller* than the computed value; a similar trend was observed recently in aldofuranosyl rings,[69] although the percent difference was estimated to be smaller (∼5%). These correction factors presumably account for the limitations of the computational method, which include the appropriateness of the adopted functional, the incompleteness of the chosen basis set, and the omission of solvent effects from the calculation. *Correction factors of +5% and −10% were applied to the coupling data in Table 9*, and these corrected couplings are plotted in Figure 1; in these plots, ±0.3 Hz errors were assigned to each data point.

Data in the $^3J_{COCH}$ plot (Figure 1A) are confined mainly to torsion angles between 20−50°, and suggest a coupling of ∼6.4 Hz for $\Theta = 0°$ and ∼8 Hz for $\Theta = 180°$. The calculated and experimental[6,7] results are in reasonable agreement, although larger couplings are calculated at the extreme dihedral angles.

Data in the $^3J_{COCC}$ plot (Figure 1B) are distributed more evenly and suggest couplings of ∼1.5 Hz for $\Theta = 60°$, near zero for $\Theta = 100°$, and ∼4.0 Hz for $\Theta = 180°$. The data point in Figure 1B associated with the $^3J_{C1,C5'}$ value in the 60*S* rotamer of **58** (3.4 Hz, Table 9, *corrected*) is correlated with a dihedral angle of 134.9° but is *larger* than the 2.2 Hz value (*corrected*) for the $^3J_{C1,C3'}$ value in 60*R* which is correlated with a *larger* dihedral angle (141.3°, Table 9). We attribute the enhanced $^3J_{C1,C5'}$ value *to the in-plane effect of O5′*. In the 60*S* conformation, O5′ lies approximately in the C1−O1−C4′−C5′ plane, and on the basis of the above-noted effects of terminal electronegative substituents on $^3J_{COCC}$, this geometry is expected to enhance coupling.

8. Other $^{13}C-^{13}C$ Spin-Coupling Constants in Saccharides. Aldopyranosyl Rings. In **37**−**44**, values of $^2J_{C1,C3}$ range from 3.9 to 4.7 Hz in β-anomers and is positive in sign[8a] (Table 5), while $^2J_{C1,C3}$ is small or zero in the α-anomers. In contrast, the $^2J_{C1,C5}$ value is large in the α-anomers (2.0−2.1 Hz) and negative in sign,[8b] whereas the $^2J_{C1,C5}$ value is small or zero in the β-anomers. In addition, the $^2J_{C2,C4}$ value is large (2.7−3.0 Hz and negative in sign)[8a,20] in configurations having O2 and O4 equatorial (**37**−**40**), whereas the $^2J_{C2,C4}$ value is small or zero when one of the terminal oxygens is axial (**41**−**44**).

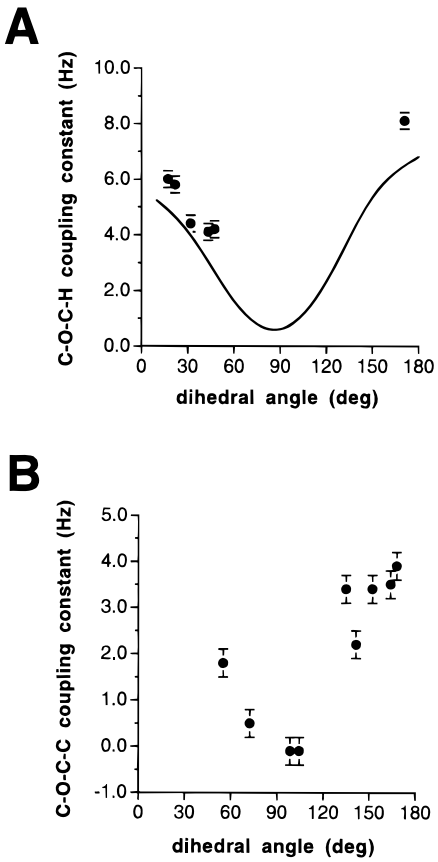

Figure 1. (A) Computed trans-*O*-glycosidic $^3J_{COCH}$ values (corrected) for dihedral angles found in geometrically optimized forms of the model disaccharide **58** (data in Table 9); error bars, ±0.3 Hz. The solid curve is the Karplus relationship for $^3J_{COCH}$ in carbohydrates reported previously.[6,7] (B) Computed trans-*O*-glycosidic $^3J_{COCC}$ values (corrected) for dihedral angles found in geometrically optimized forms of the model disaccharide **58** (data in Table 9); error bars, ±0.3 Hz.

Recent studies of $^3J_{CCCC}$ and $^3J_{COCC}$ values in aldohexopyranosyl rings have shown that *both are positive in sign*,[8b] and the observed $^{3+3}J_{C1,C4}$ and $^{3+3}J_{C2,C5}$ values are expected to be the algebraic sum of the couplings arising from their constituent $^3J_{CCCC}$ and $^3J_{COCC}$ pathways.[10] In most ring configurations, $^{3+3}J_{C1,C4}$ and $^{3+3}J_{C2,C5}$ values are very small or zero,[71] leading to the conclusion that coupling along each constituent pathway must be small or zero. Thus, the constituent $^3J_{COCC}$ pathway, which corresponds to a C1−O5−C5−C4 dihedral angle of ∼60°, must be close to zero. This conclusion contrasts with experimental $^3J_{COCC}$ values measured in **47** and **48** (Table 6), and computed the $^3J_{COCC}$ value in **58** (Figure 1B), where couplings >1.0 Hz are associated with C−O−C−C dihedral angles of ∼60°.

In contrast to previous reports,[70,71] nonzero $^{3+3}J_{C1,C4}$ values of ∼0.7 Hz are observed in aldopyranosyl rings having the α-*manno* configuration (Table 5). The +0.7 Hz coupling can be attributed to the C1−C2−C3−C4 pathway since the $^{3+3}J_{C1,C4}$ value is essentially zero in α-*gluco* isomers. While it is possible that small differences in dihedral angles within the α-*gluco* and α-*manno* rings are responsible for the measurable $^{3+3}J_{C1,C4}$ values in the latter, substantial $^{3+3}J_{C1,C4}$ values are also observed in **28** and **29** (Table 2). Thus, changes in structure at carbons along the "front" pathway can significantly affect $^{3+3}J_{C1,C4}$ in aldopyranosyl rings.

Ketohexopyranosyl Rings. $^2J_{C2,C6}$ values in ketohexopyranosyl rings are structurally related to $^2J_{C1,C5}$ values in aldopyranosyl rings. The $^2J_{C2,C6}$ value in **30** is 2.1 Hz, which is similar

in magnitude to that of $^2J_{C1,C5}$ in **34** (Table 4), indicating that substitution of a CH_2OH group for H at C1 has little effect on coupling through the C2−O6−C6 pathway.

$^3J_{C1,C4}$ values in **30**, **31**, and **33** range from 1.5 to 1.9 Hz and correspond to a C1−C2−C3−C4 dihedral angle of ∼180°.

The dual pathway coupling, $^{3+3}J_{C3,C6}$, in **30** is ∼1.6 Hz, and the related $^{3+3}J_{C2,C5}$ value in **34** is 1.8 Hz; apparently substitution of a CH_2OH for H at C2 has little effect on coupling through the constituent C3−C2−O6−C6 pathway. Thus, nonzero couplings are associated with one or both constituent pathways involving dihedral angles of ∼60°. The $^{3+3}J_{C2,C5}$ value is essentially zero in **30** and **33**, and small (∼0.7 Hz) in **31** and **32**. By comparison, the $^{3+3}J_{C1,C4}$ value is ∼0.7 Hz in α-mannopyranosyl rings, which are structurally related to **31**; this observation indicates that substitution of a CH_2OH for H at C2 has little effect on coupling through the constituent three-bond coupling pathways.

9. Construction of a $^3J_{COCC}$ Karplus Curve. Experimental $^3J_{COCC}$ data were used to construct a Karplus curve (Figure 2A); the data used to construct this plot are summarized in Table 4 of Supporting Information. The data scatter at $\Theta \approx 60°$ and 180° is caused mainly by the above-noted electronegative substituent effects. Considerably fewer experimental points are available for $\Theta < 100°$, and thus, this portion of the curve is less well defined. Combining experimental and theoretical data (from Figure 1B) improves the quality of the plot and demonstrates the high level of agreement between experimental and computed values. A partial Karplus curve (Figure 2B) constructed using coupling data in **30**, **31**, **33**, **49**, **50**, **52**, **53**, and **54** for coupling pathways involving C1 and C2 of 2-ketosugars (1AO1 or 1AO2 pathways) suggests that couplings for $\Theta \approx 180°$ are smaller (3.0−3.5 Hz) than those observed for AO21 pathways (∼4 Hz) found in aldohexopyranoses.

Least-squares fitting of a typical Karplus equation (i.e., one containing $\cos^2\Theta$ and $\cos\Theta$ terms) to the data in Figure 2A (excluding $^3J_{C1,C6}$ in ketopyranoses and couplings enhanced by in-plane oxygens) gives eq 1. This equation yields a larger ^3J

$$^3J_{COCC} = 3.70\cos^2\Theta + 0.18\cos\Theta + 0.11 \qquad (1)$$

value for $\Theta = 0°$ than for $\Theta = \pm 180°$ (Figure 2C). Interestingly, similar behavior has been suggested previously[10,11] for $^3J_{CCCC}$ along $HOH_2C-C-C-C$ pathways, with couplings of 3.5−6 Hz expected for $\Theta = 0°$ and 2−4 Hz for $\Theta = 180°$. In the present case, however, the available data for $\Theta < 100°$ are limited, thus making such a treatment uncertain. Exclusion of the cos Θ term from eq 1 and refitting the data (Figure 2C) gives the simplified equation

$$^3J_{COCC} = 3.49\cos^2\Theta + 0.16 \qquad (2)$$

This equation is better supported by the available data, but remains subject to further refinement pending the generation of more data points at $\Theta < 100°$.

10. Predicted Behavior of $^3J_{COCC}$ as a Function of the ϕ and ψ Torsion Angles in Oligosaccharides. Application of the crude $^3J_{COCC}$ Karplus curve in Figure 2C with Karplus data[6,7] for $^3J_{COCH}$ (Figure 1A) allows for the prediction of trans-*O*-glycosidic coupling behavior in an oligosaccharide containing a typical (1→4)-linkage (ϕ is defined as H1−C1−O1−CX′ and ψ is defined as C1−O1−CX′-HX′) (Figure 3). The results show that, for ϕ, $^3J_{C2,C4'}$ can be used to distinguish between the two gauche rotamers, since a larger coupling (∼4 Hz) is expected for $\phi = 60°$ than for $\phi = 300°$ (∼2 Hz). For ψ, the gauche rotamers can be similarly distinguished, noting that for $\psi = 60°$, $^3J_{C1,C5'} \approx 4$ Hz and $^3J_{C1,C3'} \approx 2$ Hz, whereas these magnitudes are reversed when $\psi = 300°$ ($^3J_{C1,C3'} \approx 4$ Hz, $^3J_{C1,C5'} \approx 2$ Hz).

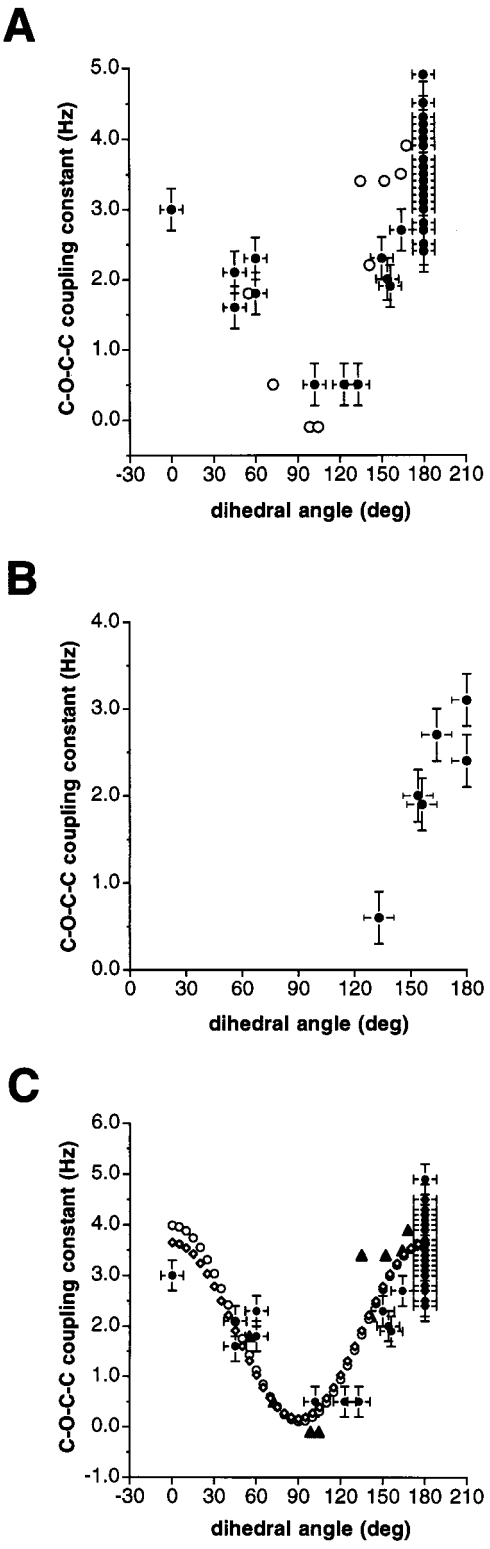

Figure 2. (A) Karplus curve for $^3J_{COCC}$ in carbohydrates derived from experimental coupling data (closed circles) (error bars, ±0.3 Hz, ±8°) and computed couplings (open circles) in Table 9. (B) Karplus curve derived for $^3J_{COCC}$ values from coupling pathways involving C1 and C2 of 2-ketosugars (1AO1 or 1AO2 pathways) (compounds **30**, **31**, **33**, **49**, **50**, **52**−**54**); error bars, ±0.3 Hz, ±8°. (C) Experimental (closed circles) and computed (closed triangles) data shown in (A) fit to eq 1 (open circles) and eq 2 (open diamonds).

The biphasic character of each curve in Figure 3 poses

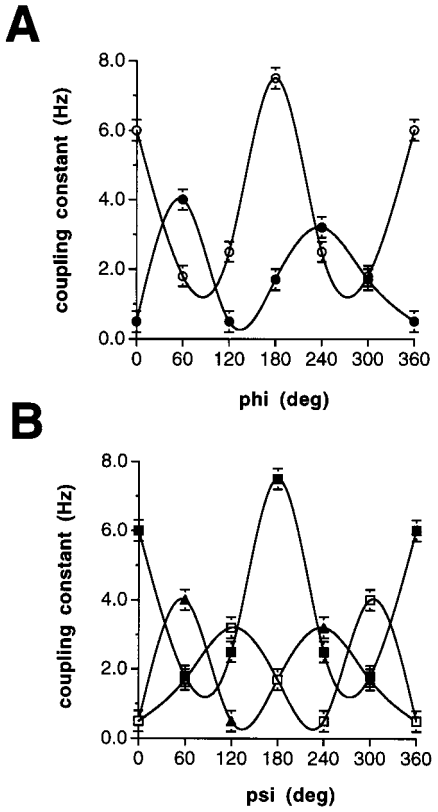

Figure 3. (A) Correlation between the glycosidic torsion angle ϕ and the two trans-*O*-glycosidic vicinal couplings ($^3J_{C2,C4'}$, closed circles; $^3J_{C4',H1}$, open circles) that are sensitive to this torsion angle. (B) Correlation between the glycosidic torsion angle ψ and the three trans-*O*-glycosidic vicinal couplings ($^3J_{C1,H4'}$, closed squares; $^3J_{C1,C3'}$, open squares; $^3J_{C1,C5'}$, closed triangles) that are sensitive to this torsion angle. Error bars, ±0.3 Hz.

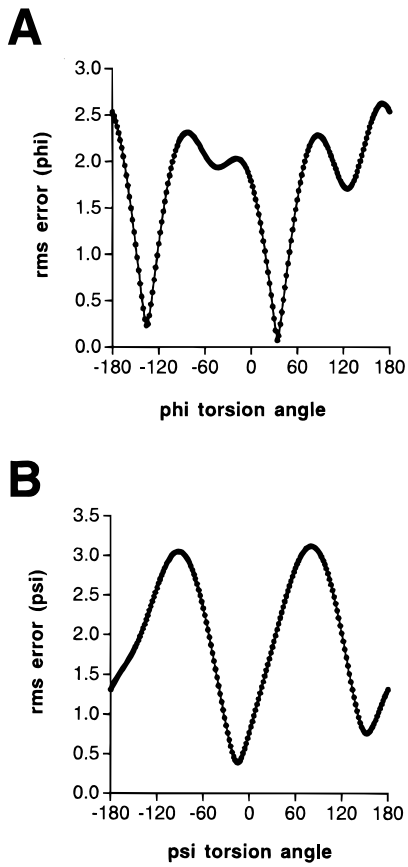

Figure 4. Root mean square errors [rms $(\theta) = \sqrt{(\Sigma_{i\to n}\ (J_{calc,i}(\theta) - J_{obs,i}(\theta))^2)/n)}$] for the trans-*O*-glycosidic couplings observed in methyl β-lactoside **1** for the ϕ (A) and ψ (B) glycosidic torsion angles. The minima at $\phi \approx 40°$ and $\psi \approx -15°$ corresponds to the torsion angles observed in the crystal structure of β-lactose.[73]

Scheme 11

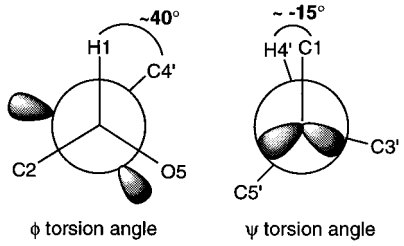

limitations on their use. For these reasons, the analysis of a single trans-*O*-glycosidic coupling for ϕ and ψ is insufficient to assign linkage conformation, especially when torsional averaging is suspected. Ideally, all five vicinal couplings and the single $^2J_{COC}$ value should be determined in order to maximize redundancy and permit a reasonable test of potential conformational models that are consistent with the available data.

11. $^3J_{COCC}$ Values in Disaccharides. Previous studies[4] of ^{13}C-labeled **1** yielded the following trans-*O*-glycosidic couplings: for ϕ, $^3J_{C4',H1} = 3.8$ Hz and $^3J_{C2,C4'} = 3.1$ Hz; for ψ, $^3J_{C1,H4'} = 4.9$ Hz, $^3J_{C1,C3'} \approx 0$ Hz, and $^3J_{C1,C5'} = 1.6$ Hz. Using these data, ϕ and ψ were predicted to be $\sim 40°$ and $\sim -15°$, respectively (ϕ is defined as H1−C1−O1−C4′ and ψ is defined as C1−O1−C4′−H4′) (Scheme 11). The 3.1 Hz value for $^3J_{C2,C4'}$ is consistent with $\Theta \approx 160°$ (Figure 2C); likewise, the 3.8 Hz value for $^3J_{C4',H1}$ suggests $\Theta \approx 40°$ (Figure 1A). With regard to ψ, the $^3J_{C1,C3'}$ value of ~0 Hz is consistent with $\Theta = 90-100°$ (Figure 2C). Of the two possible orientations, that having C1 gauche to H4′ is consistent with $^3J_{C1,H4'}$ (4.9 Hz) for $\Theta \approx 15°$ (Figure 1A). This orientation positions C1 at an ~135° dihedral angle with respect to C5′, which is consistent with the observed 1.6 Hz coupling between these nuclei; note that in this geometry, O5′ lies in the C1−O1−C4′−C5′ coupling plane, which is expected to *enhance* the observed coupling. Thus, the coupling data support one highly favored conformation about the glycosidic linkage of **1** (Scheme 11), reaffirming conclusions drawn earlier;[4] this solution geometry is similar to that observed in the crystal structure of β-lactose.[73]

When more than one coupling constant is measured for a given torsion angle, such as is found for ϕ and ψ in **1**, it can be difficult and/or misleading to fit the data visually. The root mean square deviation of all couplings plotted against torsion angle yields curves containing low-lying valleys in areas of best fit. Valleys are observed when a single conformation is consistent with the coupling data, *but their existence does not exclude the possibility of conformational averaging.* Nevertheless, this treatment is useful, as shown for **1** in Figure 4. These data show that two conformations about ϕ and ψ are consistent with the coupling data and that additional information is needed to distinguish between the two structures. For **1**, one combination of minima in each plot corresponds to the X-ray structure ($\phi \approx 40°$, $\psi \approx -15°$); other structural information is required to eliminate the remaining three combinations of minima.

Trans-*O*-glycosidic couplings in sucrose **54** are inconsistent with the crystal structure (defined as S1),[64] and computational

(73) Hirotsu, K.; Shimada, A. *Bull. Chem. Soc. Jpn.* **1974**, *47*, 1872−1879.

Scheme 12

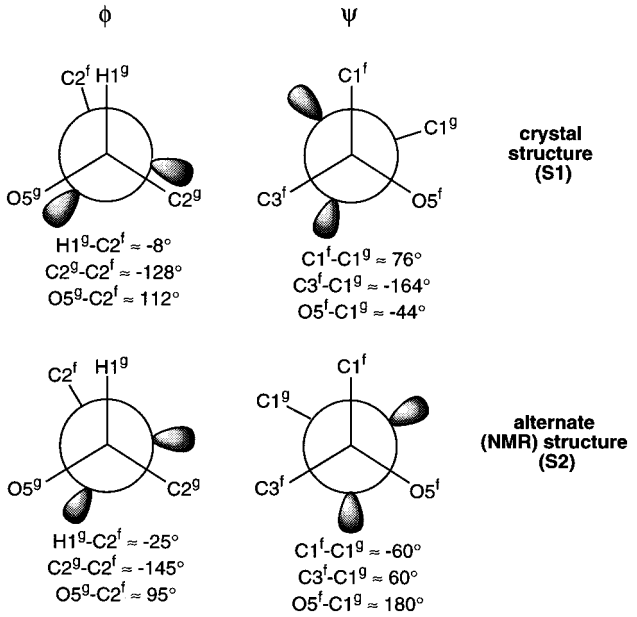

studies have suggested that an alternate low-energy structure (S2) may be present in solution.[74] In **54**, ϕ is defined as O5^g−C1^g−O1^g−C2^f and ψ is defined as C1^g−O1^g−C2^f−O5^f (the g and f superscripts denote *gluco* and *fructo* atoms, respectively). Recent measurements[5] of trans-*O*-glycosidic couplings in ^{13}C-labeled **54** give the following data: for ϕ, $^3J_{C2f,H1g} = 3.9$ Hz and $^3J_{C2f,C2g} = 2.1$ Hz; for ψ, $^3J_{C1f,C1g} = \sim 0.8$ Hz, and $^3J_{C3f,C1g} = 1.2$ Hz. Data for ϕ are consistent with both S1 and S2 (Scheme 12), with $\phi \approx 95-115°$. However, coupling data for ψ are inconsistent with S1. Couplings between C1^g−C1^f and C1^g−C3^f are expected to differ significantly in this rotamer, but similar small couplings are observed. Thus, mobility about this linkage is suspected, possibly assuming the alternate geometry shown in Scheme 12. Here the dihedral angles between C1^g−C1^f and C1^g−C3^f are similar, and similar small couplings are expected. Averaging between the crystal (S1) and alternate (S2) geometries may also account for the observed data, and indeed, recent calculations suggest that these two linkage geometries are both significantly populated in solution.[74b]

Conclusions

$^3J_{COCC}$ values have been obtained in a range of ^{13}C-labeled carbohydrates containing C−O−C−C coupling pathways having different structures and dihedral angles. The data show that factors in addition to dihedral angle affect coupling magnitude, the most critical being the disposition of terminal electronegative substituents. Thus, for OH−C−O−C−C−OH pathways, coupling between the terminal carbons will be enhanced when the terminal oxygens lie in the C−O−C−C plane ($\Theta = 180°$). Similar effects are observed for $\Theta = 60°$ when a terminal oxygen lies in-plane (HO−C−O−C or O−C−C−OH plane). Out-of-plane terminal oxygen substituents and oxygen substituents on internal carbons appear to exert little effect on coupling magnitude; thus, $^3J_{CC}$ in a $H_3C-C-O-C-OH$ pathway is virtually identical to $^3J_{CC}$ in a $HOH_2C-C-O-C-OH$ pathway *when the hydroxymethyl oxygen in the latter lies out of the C−O−C−C plane*. Similar terminal electronegative substituent effects were reported previously by Barfield and co-workers in studies of C−C−C−CH_2OH pathways;[11] the couplings observed for this pathway are similar to those observed for the C−O−C−C pathway in this work, suggesting that the in-pathway oxygen and oxygens appended to internal carbon(s) do not exert a significant influence on coupling magnitude. While terminal substituent effects could complicate the interpretation of trans-*O*-glycosidic $^3J_{COCC}$ values, they appear consistent in magnitude (~0.6 Hz per in-plane terminal oxygen) and thus should be readily accounted for in these studies. In addition, $^3J_{COCC}$ may prove valuable in assessing other structural features in saccharides, such as hydroxymethyl conformation in aldohexopyranosyl rings. In the latter regard, C−O−C−C dihedral angle and O1 disposition are constants, and thus, the only structural variable affecting $^3J_{C1,C6}$ (and $^3J_{C3,C6}$) is the C5−C6 torsion angle.

Given the importance of terminal electronegative substituents on $^3J_{CC}$ magnitude, it is useful to consider when these effects occur in trans-*O*-glycosidic C−O−C−C coupling pathways in oligosaccharides. Five glycosidic linkages are possible, 1→1, 1→2, 1→3, 1→4, and 1→6 (Scheme 13), involving simple (unsubstituted) aldohexopyranosyl rings, and in-plane oxygen substituents are encountered in the instances summarized in Table 11. It will be important to recognize and account for these structural motifs when attempting to interpret $^3J_{COCC}$ values

Scheme 13

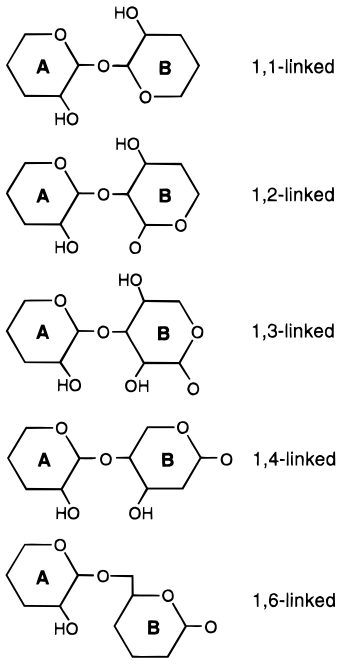

Table 11. In-Plane Geometries Involving Oxygen in Oligosaccharides

oxygen	ring[a]	coupling pathway	structural requirement
O5	A	C1−O1−CX′-CY′	ϕ rotamer = $t'g'$ [b]
O2	A	C2−C1−O1−CX′	C1−O1 and C2−O2 bonds axial
O5′	B	C1−O1−C4′−C5′	C4′−O1 bond equatorial (1,4-linkages)[b]
	B	C1−O1−C6′−C5′	C5′−C6′ rotamer = *tg* (1,6-linkages)[b]
	B	C1−O1−C2′−C1′	C2′−O1 bond equatorial (1,2-linkages)[b]
OY′ [c]	B	C1−O1−CX′-CY′	CX′−O1 and CY′-OY′ bonds axial[b]

[a] See Scheme 13 for ring assignments. [b] Relevant for both α- and β-linkages. [c] Oxygen substituents on carbons adjacent to the glycosidic linkage on Ring B.

(74) (a) Tran, V. H.; Brady, J. W. *Biopolymers* **1990**, *29*, 961−976. (b) Immel, S.; Lichtenthaler, F. W. *Liebigs Ann.* **1995**, 1925−1937.
(75) Bock, K.; Pedersen, C. *Adv. Carbohydr. Chem. Biochem.* **1983**, *41*, 27−66.
(76) Dowd, M. K.; French, A. D. *Carbohydr. Res.* **1994**, 264, 1−19.

across *O*-glycosidic linkages that differ in anomeric configuration and in the configurations of the residues involved in the linkage.

$^3J_{C1,C6}$ values in aldohexopyranosyl rings and ketohexopyanosyl rings do not obey the same Karplus relationship (Figure 2); the Karplus curve for the latter appears to have reduced amplitude. While the C1−C2−O6−C6 pathway in ketohexopyranosyl rings was initially considered to mimic the C2−C1−O1−CX′ pathway in *O*-glycosidic linkages involving aldopyranosyl rings (Scheme 3), both experimental and theoretical couplings suggest otherwise. The available data indicate that the Karplus curves for the C1−O1−CX′-CY′ and C2−C1−O1−CX′ pathways are similar.

The Karplus curves shown in Figure 2 suffer from a lack of experimental data for $\Theta = 0°$ and 60° in comparison to data for $\Theta = 180°$. This situation makes it difficult to fit the data reliably to a Karplus equation, and thus, only a simple equation has been proposed (eq 2). However, the data indicate that $^3J_{COCC}$ values for $\Theta = 0°$ and 60° lie near 3−3.5 Hz and 1−1.5 Hz, respectively. Further refinement of these curves will evolve from additional calculational studies of $^3J_{COCC}$ behavior since the present work has demonstrated that $^3J_{COCC}$ values can be computed reliably.

In summary, this investigation provides new experimental and theoretical treatments of $^3J_{COCC}$ (and $^2J_{COC}$) in carbohydrates which should facilitate their application in oligosacharide conformational analysis. Present efforts in this laboratory are directed at experimental and computational studies of biologically relevant ^{13}C-labeled di- and trisaccharides where different linkage conformations are expected. These investigations will enlarge the present database of $^2J_{COC}$ and $^3J_{COCC}$ values across *O*-glycosidic linkages and allow a more thorough test of their utility as conformational probes.

Acknowledgment. This work was supported by a grant from Omicron Biochemicals, Inc., of South Bend, Indiana, and by the Office of Basic Energy Sciences of the United States Department of Energy. This is Document No. NDRL-4054 from the Notre Dame Radiation Laboratory. R.S. wishes to thank Knut och Alice Wallenbergs Stiftelse for financial support.

Supporting Information Available: Tables (4) containing structural (selected bond lengths, angles and torsions) and conformational energies for geometrically optimized model compounds **55**−**58** obtained from DFT calculations, data used to generate Figure 2A, and schemes (2) showing molecular models of geometrically optimized structures of **55**, **56**, and **58** (10 pages, print/PDF). See any current masthead page for ordering information and Web access instructions.

JA981127F